

Effects of uniaxial strain in LaMnO_3

K. H. Ahn* and A. J. Millis

Center for Materials Theory

Department of Physics and Astronomy, Rutgers University

Piscataway, New Jersey 08854

Abstract

The effects of uniaxial strain on the structural, orbital, optical, and magnetic properties of LaMnO_3 are calculated using a general elastic energy expression, along with a tight-binding parameterization of the band theory. Tensile uniaxial strain of the order of 2 % (i.e., of the order of magnitude of those induced in thin films by lattice mismatch with substrates) is found to lead to changes in the magnetic ground state, leading to dramatic changes in the band structure and optical conductivity spectrum. The magnetostriction effect associated with the Neel transition of bulk(unstrained) LaMnO_3 is also determined. Due to the Jahn-Teller coupling, the uniform tetragonal distortion mode is softer in LaMnO_3 than in doped cubic manganates. Reasons why the observed $(\pi\pi 0)$ orbital ordering is favored over a $(\pi\pi\pi)$ periodicity are discussed.

71.38.+i, 75.70.Ak, 72.15.Gd, 75.80.+q

I. INTRODUCTION

The ‘colossal’ magnetoresistive manganese perovskites have been a focus of recent attention.¹ Since most of the technological applications require thin films on substrates, it is important to understand the effects of strains induced by substrates. Because Mn e_g electrons, which determine important physical properties of these materials, are coupled to the lattice degrees of freedom through the Jahn-Teller (JT) coupling, it is expected that uniaxial or biaxial strains are important and that even relatively small strains may result in observable effects on the electronic properties of these materials. Recently, the effects of substrate-induced strains on the properties of thin manganate films have been studied experimentally.^{2,3} It is indeed found that the ferromagnetic and metal-insulator transition temperature, T_c , depends sensitively on the volume-preserving uniaxial strains, as do the magnetic anisotropy, magnetoresistance, and charge ordering transition.

In this work, we study the effects of uniaxial strains in LaMnO_3 , which is the parent compound of the doped manganese perovskites. Our motivations are to further clarify the properties of this interesting compound and to test techniques and fix parameters so the more complicated behaviors of the doped compounds may be studied. At very high temperatures, bulk LaMnO_3 exists in cubic perovskite structure, but at $T < 750$ K, it has a static $(\pi, \pi, 0)$ $3x^2 - r^2/3y^2 - r^2$ type Jahn-Teller distortion.⁴ It also has a uniform tetragonal distortion, which originates from the coupling of the staggered and uniform distortions by an anharmonic elastic energy.⁵ This coupling implies that the substrate-induced strain may affect the orbital ordering.

In Ref. 6, following Kanamori, a model with harmonic Mn-O and Mn-Mn elastic forces and a local anharmonic energy term was used to study lattice distortions in this material. It predicted (π, π) type ordering in xy plane as observed in LaMnO_3 . However, according to this model, $(\pi, \pi, 0)$ and (π, π, π) type orderings have the same energy. The reason why $(\pi, \pi, 0)$ ordering is favored has not been understood so far. Bulk LaMnO_3 has so called A-type antiferromagnetic (AF) ordering below 140 K, in which spins align parallel in xy plane and antiparallel along z direction.⁴ This peculiar spin ordering pattern is the result of the exchange interaction between Mn ions which depends on the e_g orbital ordering as explained in Ref. 7. Indications of a coupling between orbital ordering and magnetic ordering have also been found in a recent X-ray resonant scattering experiment.⁸

In this paper, we present more general expressions for the elastic energy than those in Ref. 6. We use these to study the ground state energy and distortions in bulk state, and the effects of uniaxial strains in thin films. We also present a simple model of the magnetic interaction depending explicitly on the orbital states, and we use this to study the magnetostriction effects in bulk state and the change of the magnetic interaction due to the strains in thin films. We examine the changes in the band structure and optical conductivity due to the strains, using a nearest-neighbor tight binding approximation. We also compare the energies of $(\pi, \pi, 0)$ and (π, π, π) type orderings, and examine why the observed $(\pi, \pi, 0)$ distortion is favored over the (π, π, π) type distortion. Our calculations suggest that 2 % tensile strain can change the observed A-type(layered) antiferromagnetic state into a purely antiferromagnetic state. This change would induce large changes in band structure and optical conductivity spectrum, which we calculate. Finally, we show that the magnetostriction effect at the Neel transition is large.

The rest of the paper is organized in the following way. Section II introduces a model of elastic energy, Sect. III a model of the magnetic interaction and magnetostriction effect, and Sect. IV a tight binding model for band structure and optical conductivity. Section V compares the ground state energies of $(\pi, \pi, 0)$ and (π, π, π) type distortions. Section VI presents the results. Section VII summarizes the main conclusions. In Appendices A and B, we show how we determine general expressions of the elastic energy, and how we determine the parameters, respectively.

II. MODEL OF LATTICE ENERGY

A. Overview

To study the effects of uniaxial strains in thin films, we first need to understand the strains already present in bulk state. The elastic energy depends on three important variables: the oxygen displacement along Mn-Mn direction, the three-dimensional Mn ion displacement, and the Mn e_g electron orbital state.^{5,6} More precisely, the degrees of freedom we will consider are defined in the following way: In the ideal cubic perovskite structure with lattice constant a_0 , the Mn ions are located at $a_0\vec{i}$, and oxygen ions at $a_0(\vec{i} + \hat{a}/2)$, where i_x , i_y , and i_z are integers and $\hat{a}=\hat{x}$, \hat{y} , and \hat{z} . We write the displacement of Mn at $a_0\vec{i}$ as $a_0(\vec{e} \cdot \vec{i} + \vec{\delta}_i)$, where $\vec{\delta}_i$ represents nonzero-wavevector Mn-ion displacement, $\vec{e} = e_{xx}\hat{x} + e_{yy}\hat{y} + e_{zz}\hat{z}$, and e_{ij} is the conventional strain tensor referred to the ideal cubic perovskite lattice (we need only the diagonal components). The displacement of oxygen at $a_0(\vec{i} + \hat{a}/2)$ along Mn-Mn axis is $a_0[\vec{e} \cdot (\vec{i} + \hat{a}/2) + u_i^a\hat{a}]$, where u_i^a represents O-ion displacement with nonzero wavevector. Figure 1 shows $\vec{\delta}_i$ and $u_i^{x,y,z}$. We assume that we have already minimized the elastic energy over the displacements of O ions perpendicular to the Mn-Mn axis and the displacement of La ions. Therefore, even though we do not consider the buckling of the Mn-O-Mn bond explicitly, its effect is implicitly included in our harmonic and anharmonic elastic constants below.

We treat the elastic energy due to these strains in up to cubic anharmonic terms, and the coupling of the strain to the Mn e_g orbital state by the Jahn-Teller coupling. In this paper, instead of representing the elastic energy in terms of spring constants between different ions as done in Refs. 5 and 6, we will introduce a more general and, we hope, more useful formulation in which long wavelength lattice distortions are treated via conventional elastic theory, while the short wavelength atomic motions are treated explicitly.

B. General energy expressions for $(\pi, \pi, 0)$ and (π, π, π) distortions

The energy per Mn ion due to uniform strains, e_{xx} , e_{yy} , and e_{zz} , is most conveniently written in terms of the following combinations:

$$Q_{1u} = \frac{a_0}{\sqrt{3}}(e_{xx} + e_{yy} + e_{zz}), \quad (1)$$

$$Q_{2u} = \frac{a_0}{\sqrt{2}}(e_{xx} - e_{yy}), \quad (2)$$

$$Q_{3u} = \frac{a_0}{\sqrt{6}}(2e_{zz} - e_{xx} - e_{yy}). \quad (3)$$

We have

$$\frac{E_u}{N_{Mn}} = \frac{1}{2}K_B Q_{1u}^2 + \frac{1}{2}K^*(Q_{2u}^2 + Q_{3u}^2), \quad (4)$$

where the bulk modulus $K_B = a_0(c_{11} + 2c_{12}) = 3a_0c_B$, the Jahn-Teller shear modulus $K^* = a_0(c_{11} - c_{12}) = 2a_0c^*$, and c_{ij} are the usual elastic constants.

In addition to these uniform strains, we consider staggered distortions with wave vector $\vec{k} = (\pi, \pi, 0)$ or (π, π, π) . We represent the amplitudes of the distortions by $a_0\vec{\delta}_{\vec{k}}$ for Mn ions and $a_0u_{\vec{k}}^{x,y,z}$ for O ions. Translational symmetry implies that the uniform distortion and the staggered distortion do not couple with each other up to the second order. Therefore, the harmonic elastic energy due to the staggered distortions simply adds to the harmonic uniform strain energy. In Appendix A, we use symmetry arguments to obtain the general forms of the elastic energies due to $\vec{\delta}_{\vec{k}}$ and $u_{\vec{k}}^{x,y,z}$ for $(\pi, \pi, 0)$ and (π, π, π) distortions. In the Jahn-Teller coupling energy E_{JT} , which we will introduce later, only the lattice distortions which have even parity about Mn ions appear. Therefore, E_{JT} does not depend on the Mn-distortions $\delta_{\vec{k}}^{x,y,z}$ for either $\vec{k} = (\pi, \pi, 0)$ or $\vec{k} = (\pi, \pi, \pi)$, or the z-direction oxygen distortion $u_{\vec{k}}^z$ for $\vec{k} = (\pi, \pi, 0)$. The energy cost of the relevant distortions is most conveniently written in terms of

$$Q_{2s} = \frac{a_0}{\sqrt{2}}(v_{sx} - v_{sy}), \quad (5)$$

$$Q_{3s} = \frac{a_0}{\sqrt{6}}(2v_{sz} - v_{sx} - v_{sy}), \quad (6)$$

where v_{sa} is the $(\pi\pi 0)$ or $(\pi\pi\pi)$ amplitude of $v_i^a = u_i^a - u_{i-\hat{a}}^a$. The energy of a staggered distortion, E_s , depends upon the ordering wavevector and, for the distortions we consider, is

$$\frac{E_s(\pi, \pi, 0)}{N_{Mn}} = \frac{1}{2}K_{2s}Q_{2s}^2 + \frac{1}{2}K_{3s}Q_{3s}^2, \quad (7)$$

$$\frac{E_s(\pi, \pi, \pi)}{N_{Mn}} = \frac{1}{2}K_s(Q_{2s}^2 + Q_{3s}^2), \quad (8)$$

where the K_{2s} , K_{3s} , and K_s are the elastic constants defined in Appendix A, and arise mainly from the Mn-O bond stretching mode.⁹

We compare the sizes of K^* , K_{2s} , K_{3s} , and K_s . This comparison is important to determine the ground state distortions. A uniform strain changes more bonds than a staggered distortion. For example, within a harmonic nearest-neighbor approximation, Q_{2s} and Q_{3s} modes involve only the Mn-O bond, but Q_{2u} and Q_{3u} modes involve both Mn-O and Mn-Mn bonds. Therefore, uniform modes have larger elastic moduli than staggered modes, which remains true when reasonable further neighbor interactions are included. Therefore, we expect $K^* > K_{3s}$, K_{2s} , K_s . Our analysis of the general expression of the elastic energy given in Appendix A shows $K_{3s} > K_{2s}$.

The staggered lattice distortion is caused by the Jahn-Teller coupling to the Mn e_g orbital state. The Mn e_g electron state on site $a_0\vec{i}$ is represented by

$$|\theta_{\vec{i}}\rangle = \cos\theta_{\vec{i}}|3z^2 - r^2\rangle + \sin\theta_{\vec{i}}|x^2 - y^2\rangle, \quad (9)$$

where $|3z^2 - r^2\rangle$ and $|x^2 - y^2\rangle$ are the two linearly independent e_g orbitals on the site. The cases of interest here are two-sublattice distortions. We represent the orbital states of e_g electrons on these two sublattices as θ_1 and θ_2 . Then the JT energy is^{5,6}

$$\frac{E_{JT}}{N_{Mn}} = -\sqrt{\frac{3}{2}}\lambda\frac{1}{2}[\cos 2\theta_1(Q_{3u} + Q_{3s}) + \sin 2\theta_1(Q_{2u} + Q_{2s}) + \cos 2\theta_2(Q_{3u} - Q_{3s}) + \sin 2\theta_2(Q_{2u} - Q_{2s})]. \quad (10)$$

To represent the energy only in terms of lattice distortions, we minimize the above Jahn-Teller energy with respect to the orbital states θ_1 and θ_2 . We obtain

$$\cos 2\theta_{1,2}^{\min} = \frac{Q_{3u} \pm Q_{3s}}{\sqrt{(Q_{2u} \pm Q_{2s})^2 + (Q_{3u} \pm Q_{3s})^2}}, \quad (11)$$

$$\sin 2\theta_{1,2}^{\min} = \frac{Q_{2u} \pm Q_{2s}}{\sqrt{(Q_{2u} \pm Q_{2s})^2 + (Q_{3u} \pm Q_{3s})^2}}, \quad (12)$$

and

$$\frac{E_{JT}}{N_{Mn}} = -\frac{1}{2}\sqrt{\frac{3}{2}}\lambda\left[\sqrt{(Q_{2u} + Q_{2s})^2 + (Q_{3u} + Q_{3s})^2} + \sqrt{(Q_{2u} - Q_{2s})^2 + (Q_{3u} - Q_{3s})^2}\right]. \quad (13)$$

We also include the largest anharmonic energy, which is the one between the nearest neighbor Mn-O pair. It is given by

$$E_{anh} = \frac{4}{\sqrt{3}}Aa_0^3\sum_{i,a}\left(\frac{e_{aa}}{2} + u_i^a - \delta_i^a\right)^3 + \left(\delta_i^a - u_{i-a}^a - \frac{e_{aa}}{2}\right)^3. \quad (14)$$

Total energy is the sum of the terms considered so far:

$$E_{tot}^{elastic} = E_u + E_s + E_{JT} + E_{anh}. \quad (15)$$

By minimizing $E_{tot}^{elastic}$, we find the distortions induced by the JT coupling and anharmonic energy terms, which will be discussed below for $\vec{k} = (\pi, \pi, 0)$ and $\vec{k} = (\pi, \pi, \pi)$ distortions separately.

C. Energy minimization for $(\pi, \pi, 0)$ distortion

We minimize $E_u + E_s + E_{JT}$ and then treat E_{anh} as a perturbation, since we expect and will show below that the anharmonic term is small compared to the harmonic terms. We find that in the ground state of $E_u + E_s + E_{JT}$, the distortion mode which has the smallest

modulus among Q_{2u} , Q_{3u} , Q_{2s} , and Q_{3s} is non-zero, and all the other distortion modes vanish. Since, we found $K^* > K_{3s} > K_{2s}$, the ground state of $E_u + E_s + E_{JT}$ is

$$Q_{3s} = Q_{2u} = Q_{3u} = 0, \quad (16)$$

$$Q_{2s} = \sqrt{\frac{3}{2}} \frac{\lambda}{K_{2s}}, \quad (17)$$

$$E_{\min} = -\frac{3}{4} \frac{\lambda^2}{K_{2s}}, \quad (18)$$

$$\theta_1, \theta_2 = \pi/4, 3\pi/4. \quad (19)$$

It is noteworthy that in this ground state the Mn lattice itself preserves cubic symmetry, and only oxygen ions make staggered distortions.

We next study how the anharmonic energy term changes the above ground state. We represent E_{anh} in Eq. (14) by $\vec{\delta}_{\vec{k}}$, $u_{\vec{k}}^{x,y,z}$, and $e_{xx,yy,zz}$. Direct expansion (or symmetry argument) shows that each of $\vec{\delta}_{\vec{k}}$ and $u_{\vec{k}}^z$ appears only as the second order in E_{anh} , which implies that these distortions remain zero unless the coupled uniform strains exceed certain values and the lattice becomes unstable. After representing $E_{anh}(\pi\pi0)$ in terms of $Q_{1u,2u,3u,2s,3s}$, the same argument shows $Q_{3s} = Q_{2u} = 0$. By taking the largest remaining term, we obtain¹⁰

$$\frac{E_{anh}(\pi\pi0)}{N_{Mn}} \approx A Q_{2s}^2 (Q_{1u} - \frac{1}{\sqrt{2}} Q_{3u}). \quad (20)$$

The total energy for $\vec{k} = (\pi, \pi, 0)$ distortion which we will minimize to find strains in bulk state or in thin films is

$$\begin{aligned} E_{\text{tot}}(\pi\pi0) &= (E_u + E_s + E_{JT} + E_{anh})/N_{Mn} \\ &= \frac{1}{2} K_B Q_{1u}^2 + \frac{1}{2} K^* Q_{3u}^2 + \frac{1}{2} K_{2s} Q_{2s}^2 - \sqrt{\frac{3}{2}} \lambda \sqrt{Q_{2s}^2 + Q_{3u}^2} + A Q_{2s}^2 \left(Q_{1u} - \frac{1}{\sqrt{2}} Q_{3u} \right). \end{aligned} \quad (21)$$

In bulk state, there is no external constraint. When we minimize $E_{\text{tot}}(\pi\pi0)$ in a leading order in A to find the lattice distortions in the bulk state, we obtain

$$E_{\text{tot}}^{MIN}(\pi\pi0) = -\frac{3}{4} \frac{\lambda^2}{K_{2s}} - A^2 \frac{9}{16} \frac{\lambda^4}{K_{2s}^4} \frac{2K^* - 2K_{2s} + K_B}{K_B(K^* - K_{2s})} + O(A^4), \quad (22)$$

for

$$Q_{1u} = -\frac{3}{2} \frac{\lambda^2}{K_{2s}} \frac{A}{K_{2s}^2} + O(A^3), \quad (23)$$

$$Q_{2s} = \sqrt{\frac{3}{2}} \frac{\lambda}{K_{2s}} + O(A^2), \quad (24)$$

$$Q_{3s} = Q_{2u} = 0, \quad (25)$$

$$Q_{3u} = \frac{3\lambda^2 A}{2\sqrt{2}(K^* - K_{2s})K_{2s}^2} + O(A^3). \quad (26)$$

The results show that the observed uniform tetragonal distortion is due to the anharmonic term which couples staggered and uniform distortions. LaMnO₃ expands upon heating, which implies $A < 0$. Therefore, above result indicates $Q_{3u} < 0$, which is consistent with the observed distortion in bulk LaMnO₃. Since $K^* - K_{2s}$ is order of magnitude smaller than K_{2s} , Q_{3u} is order of magnitude larger than Q_{1u} . Up to order of A , the anharmonic term does not change Q_{2s} .

We note “ Q_{3u} mode softening” : When we have lattice distortion $Q_{2s} = \sqrt{3/2} \frac{\lambda}{K_{2s}}$, the JT coupling term in Eq. (21), expanded about small Q_{3u} , effectively reduces Q_{3u} mode modulus by $-K_{2s}$. Therefore, when the anharmonic term induces Q_{3u} , the restoring spring constant is $K^* - K_{2s}$ rather than K^* . This is the reason why we have $K^* - K_{2s}$ in the denominator of Eq. (26) and have a relatively large Q_{3u} ($\sim 35\%$ of Q_{2s} from crystallography data). Thus we expect the shear modulus corresponding to the Q_{3u} distortion to be much smaller in LaMnO₃ than in doped cubic manganates.

D. Energy minimization for (π, π, π) distortion

By applying similar considerations to (π, π, π) distortion, and using the condition $K^* > K_s$, we find that the degenerate ground states of $E_u + E_s(\pi\pi\pi) + E_{JT}(\pi\pi\pi)$ are

$$Q_{2u} = Q_{3u} = 0, \quad (27)$$

$$Q_{2s} = \sqrt{\frac{3}{2}} \frac{\lambda}{K_s} \sin 2\theta_1, \quad (28)$$

$$Q_{3s} = \sqrt{\frac{3}{2}} \frac{\lambda}{K_s} \cos 2\theta_1, \quad (29)$$

$$E_{\min} = -\frac{3}{4} \frac{\lambda^2}{K_s}, \quad (30)$$

$$\theta_2 = \pi - \theta_1, \quad (31)$$

where θ_1 is an arbitrary angle between 0 and π . After we include the same anharmonic energy and apply the same arguments used for the $(\pi, \pi, 0)$ distortion, we find the total energy expression for the (π, π, π) distortion which we will minimize further is

$$E_{tot}(\pi\pi\pi) = [E_u + E_s(\pi\pi\pi) + E_{JT}(\pi\pi\pi) + E_{anh}(\pi\pi\pi)]/N_{Mn} \quad (32)$$

$$= \frac{1}{2} K_B Q_{1u}^2 + \frac{1}{2} K^* (Q_{2u}^2 + Q_{3u}^2) + \frac{1}{2} K_s (Q_{2s}^2 + Q_{3s}^2) \quad (33)$$

$$- \sqrt{\frac{3}{2}} \lambda \frac{1}{2} \left[\sqrt{(Q_{2u} + Q_{2s})^2 + (Q_{3u} + Q_{3s})^2} + \sqrt{(Q_{2u} - Q_{2s})^2 + (Q_{3u} - Q_{3s})^2} \right]$$

$$+ A \left[Q_{2s}^2 (Q_{1u} - \frac{1}{\sqrt{2}} Q_{3u}) + Q_{3s}^2 (Q_{1u} + \frac{1}{\sqrt{2}} Q_{3u}) - \sqrt{2} Q_{2s} Q_{3s} Q_{2u} \right].$$

When we minimize $E_{tot}(\pi\pi\pi)$, we obtain

$$E_{tot}^{MIN}(\pi\pi\pi) = -\frac{3}{4} \frac{\lambda^2}{K_s} - A^2 \frac{9}{16} \frac{\lambda^4}{K_s^4} \frac{2K^* - 2K_s + K_B}{K_B(K^* - K_s)} + O(A^4) \quad (34)$$

for

$$Q_{1u} = -\frac{3 \lambda^2 A}{2 K_s K_s^2} + O(A^3), \quad (35)$$

$$Q_{2s} = \sqrt{\frac{3}{2}} \frac{\lambda}{K_s} + O(A^2), \quad (36)$$

$$Q_{3s} = Q_{2u} = 0, \quad (37)$$

$$Q_{3u} = \frac{3\lambda^2 A}{2\sqrt{2}(K^* - K_s)K_s^2} + O(A^3). \quad (38)$$

The other two physically equivalent distortions obtained by permuting x , y , and z from above results are also degenerate ground states. The ground state energies for the $(\pi\pi 0)$ and $(\pi\pi\pi)$ distortions will be compared in Sect. V.

E. Energy minimization for strained films

In this paper, by uniaxial strain, we mean a tetragonal strain with axis perpendicular to film plane. This strain can be applied by growing epitaxial films on square lattice substrates with lattice parameters different from the xy plane lattice parameter for bulk LaMnO₃. For thin films with uniaxial strains, we calculate the lattice distortions in the following way: We assume that $(\pi\pi 0)$ distortion pattern is favored even in strained films. We also assume perfect epitaxy; therefore e_{xx} and e_{yy} are determined by substrates. Then Q_{2s} and e_{zz} for given strains can be found by minimizing E_{tot} about these distortions, which also give Q_{1u} and Q_{3u} . From Q_{2s} and Q_{3u} , we find the e_g orbital states, θ_1 and θ_2 , by

$$\cos(2\theta_1) = \frac{Q_{3u}}{\sqrt{Q_{2s}^2 + Q_{3u}^2}}, \quad (39)$$

$$\theta_2 = \pi - \theta_1. \quad (40)$$

Since the external strain changes Q_{2s} and Q_{3u} , it also changes the JT splitting, given by $\delta\Delta E_{JT} = \sqrt{6}\lambda\sqrt{Q_{2s}^2 + Q_{3u}^2} - \sqrt{6}\lambda\sqrt{(Q_{2s}^{eq})^2 + (Q_{3u}^{eq})^2}$. Parameters of the model, i.e., K_B , K^* , K_{2s} , λ , and A , are determined from experiments, as explained in Appendix B. The determined parameter values are shown in Table I.

III. MODEL OF MAGNETIC INTERACTION AND MAGNETOSTRICTION EFFECTS

A. Magnetic interaction

In this section, we present a model describing magnetism in bulk and strained films of LaMnO₃. The superexchange interaction between Mn ions in LaMnO₃ depends on the electron orbital overlap, particularly the overlap between Mn e_g orbitals and O p orbitals.¹¹ It is also argued that t_{2g} electrons also contribute antiferromagnetic interaction. We build a simple model below, which incorporates these two contributions of exchange interactions.

We calculate the superexchange interaction due to the e_g electrons using a similar method as in Ref. 7. We assume e_g spin is always parallel to t_{2g} spin at each site due to the strong Hund's coupling. For the two Mn ions, one at \vec{i} and the other at $\vec{i} + \hat{z}$, we find

$$J_{e_g}(\theta_1, \theta_2) = -J_F \left(\sin^2 \theta_1 \cos^2 \theta_2 + \cos^2 \theta_1 \sin^2 \theta_2 \right), \quad (41)$$

where J_F is a positive parameter of the model. This is, in fact, equivalent to the model in Ref. 7, if we assume that the state with two holes on the intermediate oxygen ion (which was considered in Ref. 7) requires an infinite energy. Equation (41) shows that when one of θ_1 and θ_2 is zero (i.e., $|3z^2 - r^2 >$ state) and the other is $\pi/2$ (i.e., $|x^2 - y^2 >$ state), $J_{e_g}(\theta_1, \theta_2)$ is most ferromagnetic due to the maximized hopping between the filled orbital on one site and the empty orbital on the other site. When $\theta_1 = \theta_2 = \pi/2$, or $\theta_1 = \theta_2 = 0$, $J_{e_g}(\theta_1, \theta_2)$ is least ferromagnetic, since the hopping between the filled and empty orbitals on the two sites vanishes. The t_{2g} superexchange is expected to be independent of θ_1 and θ_2 , and always antiferromagnetic, so we set $J_{t_{2g}} = J_{AF}$. Therefore, along the z direction the total exchange interaction is

$$\begin{aligned} J_z &= J_{t_{2g}} + J_{e_g} \\ &= J_{AF} - J_F \left(\sin^2 \theta_1 \cos^2 \theta_2 + \cos^2 \theta_1 \sin^2 \theta_2 \right). \end{aligned} \quad (42)$$

The sign of the total superexchange is determined by the competition between the e_g ferromagnetism and t_{2g} antiferromagnetism. Along x and y directions, proper rotations result in

$$J_x = J_{AF} - J_F \left(\sin^2 \left(\theta_1 - \frac{2\pi}{3} \right) \cos^2 \left(\theta_2 - \frac{2\pi}{3} \right) + \cos^2 \left(\theta_1 - \frac{2\pi}{3} \right) \sin^2 \left(\theta_2 - \frac{2\pi}{3} \right) \right), \quad (43)$$

$$J_y = J_{AF} - J_F \left(\sin^2 \left(\theta_1 + \frac{2\pi}{3} \right) \cos^2 \left(\theta_2 + \frac{2\pi}{3} \right) + \cos^2 \left(\theta_1 + \frac{2\pi}{3} \right) \sin^2 \left(\theta_2 + \frac{2\pi}{3} \right) \right). \quad (44)$$

Using the condition $\theta_2 = \pi - \theta_1$ obtained before, we find

$$J_x = J_y \equiv J_{xy} = J_{xy}^0 + J^* \cos 4\theta_1, \quad (45)$$

$$J_z = J_z^0 + J^* \cos 4\theta_1, \quad (46)$$

where $J_{xy}^0 = J_{AF} - 5J_F/8$, $J_z^0 = J_{AF} - J_F/4$, and $J^* = J_F/4$. It explicitly shows how the magnetic coupling depends on the orbital states.

B. Magnetostriction effects

In this section, we present our model of magnetostriction effect in bulk LaMnO₃. We expect magnetostriction effect for the following reason: Since J_x , J_y , and J_z depend on the orbital states θ_1 and θ_2 , once certain magnetic ordering occurs, the magnetic ordering, in turn, will change θ_1 and θ_2 to gain further magnetic energy. Through the JT coupling, this change in the orbital states can cause the change in the JT strains. Magnetism and lattice distortion are coupled through the Mn e_g orbital degree of freedom.

To estimate the size of the magnetostriction effects, we add to Eq. (21) the term

$$\frac{E_{mag}}{N_{Mn}} = -4(2|J_{xy}(\theta_1)| + |J_z(\theta_1)|), \quad (47)$$

which represents the mean-field $T=0$ magnetic energy, and find the changes in the orbital states. For A-type antiferromagnetic state, after dropping constant terms, we obtain

$$\frac{E_{mag}}{N_{Mn}} = 4J^* \cos 4\theta_1. \quad (48)$$

By adding E_{mag}/N_{Mn} to the total energy, we can find the extra structure at $T=0$ due to the magnetic order.

Using the Landau free energy method, we examine whether the magnetostriction effect makes the phase transition first order or not. From the energy gain due to the magnetic order at $T=0$, and the mean field estimate of T_c , we obtain the Landau free energy per site, f :

$$f(\theta_1, Q_{1u}, Q_{2s}, Q_{3u}, m) = 2[T - T_c(\theta_1)]m^2 + T_c(\theta_1)m^4 + E_{elastic}(\theta_1, Q_{1u}, Q_{2s}, Q_{3u}), \quad (49)$$

where $m = M/M(T=0)$ is the normalized magnetization and $E_{elastic}(\theta_1, Q_{1u}, Q_{2s}, Q_{3u})$ is the total elastic energy obtained in Sect. II. Magnetic ordering temperature, $T_c(\theta_1)$, can be obtained by molecular field theory:¹²

$$T_c(\theta_1) = 2(4|J_{xy}(\theta_1)| + 2|J_z(\theta_1)|). \quad (50)$$

We can find the order of the phase transition and the size of the magnetostriction effect in the following approximation: Since Q_{1u} is not directly coupled to θ_1 , we expect the change in Q_{1u} is small, which can be seen from the numerical results in Table II. Therefore, we neglect Q_{1u} dependence and obtain $E_{elastic}(\theta_1, Q_{2s}, Q_{3u})$, which we minimize further about Q_{2s} and Q_{3u} to obtain $E_{elastic}(\theta_1)$. By expanding $E_{elastic}(\theta_1)$ about the minimum energy orbital state for $m=0$, $\theta_1(m=0)$, we obtain

$$E_{elastic}(\theta_1) \approx \frac{1}{2}K_\theta (\theta_1 - \theta_1(m=0))^2, \quad (51)$$

where $K_\theta = 12\lambda^2(K^* - K_{2s})/(K_{2s}K^*)$, and $\theta_1(m=0) = \frac{1}{2}\cos^{-1}[\sqrt{3}\lambda A/(K_{2s}(K^* - K_{2s}))]$. By substituting $T_c(\theta_1) \approx T_c^0[1 + \alpha(\theta_1 - \theta_1(m=0))]$ and $E_{elastic}(\theta_1)$ in Eq. (49), and minimizing $f(\theta_1, m)$ about θ_1 , we obtain

$$\theta_1(m) - \theta_1(m=0) = \frac{1}{K_\theta} [2T_c^0\alpha m^2 - T_c^0\alpha m^4], \quad (52)$$

$$f(m) = 2(T - T_c^0)m^2 + \frac{T_c^0}{K_\theta}(K_\theta - 2\alpha^2 T_c^0)m^4 + O(m^6). \quad (53)$$

Therefore, we will have the second order phase transition when $K_\theta > 2\alpha^2 T_c^0$, and the first order transition when $K_\theta < 2\alpha^2 T_c^0$. This result implies that when the lattice is soft (small K_θ) or the coupling between magnetic interaction and lattice is large (large α), the transition becomes first-order. The estimate of the parameters for LaMnO₃ in Sect. VI.C predicts the second-order phase transition. Above equation for $\theta_1(m)$ also gives the net change of θ_1 , $\theta_1(T=0) - \theta_1(T > T_c) = \alpha T_c^0/K_\theta$.

IV. MODEL OF BAND STRUCTURE AND OPTICAL CONDUCTIVITY

We use a tight-binding approximation to calculate band structure and optical conductivity for strained films. This method is explained in detail in Ref. 13, and summarized in this section. According to band theory calculations^{14,15} the conduction band is derived mainly from the Mn e_g symmetric d-orbitals and is well separated from other bands. Therefore, we only consider Mn e_g levels. Kinetic energy and chemical potential terms are

$$H_{\text{KE}} + H_{\mu} = -\frac{1}{2} \sum_{\vec{i}, \vec{\delta}, a, b, \alpha} t_{\vec{\delta}}^{ab} d_{i\alpha}^{\dagger} d_{\vec{i}+\vec{\delta}b\alpha} + H.c. - \mu \sum_{\vec{i}, a, \alpha} d_{i\alpha}^{\dagger} d_{i\alpha}. \quad (54)$$

Here \vec{i} represents the coordinates of Mn sites, $\delta (= \pm x, y, z)$ labels the nearest neighbors of Mn sites, a and b represent the two degenerate Mn e_g orbitals on a site, α denotes the spin state, and $t_{\vec{\delta}}^{ab}$ is the hopping amplitude between orbital a on site \vec{i} and b on site $\vec{i} + \vec{\delta}$. We choose $|\psi_1\rangle = |3z^2 - r^2\rangle$ and $|\psi_2\rangle = |x^2 - y^2\rangle$ as the two linearly independent e_g orbitals on each site as before. The hopping matrix $t_{\vec{\delta}}^{ab}$ has a special form: For hopping along z direction, it connects only the two $|3z^2 - r^2\rangle$ states, thus $t_z^{ab} = t_{-z}^{ab} = t_o$ for $a=b=1$, and zero otherwise. The hopping matrices in other bond directions are obtained by appropriate rotations. The Jahn-Teller coupling for uniform Q_3 distortion and staggered Q_2 distortion with wave vector $\vec{K}_{\text{lattice}} = (\pi, \pi, 0)$ or (π, π, π) is

$$H_{\text{JT}} = -\sqrt{\frac{3}{2}}\lambda \sum_{\vec{i}, \alpha} \begin{pmatrix} d_{1, \vec{i}, \alpha}^{\dagger} \\ d_{2, \vec{i}, \alpha}^{\dagger} \end{pmatrix}^T \begin{pmatrix} -Q_{3u} & \exp(i\vec{K}_{\text{lattice}} \cdot \vec{i})Q_{2s} \\ \exp(i\vec{K}_{\text{lattice}} \cdot \vec{i})Q_{2s} & Q_{3u} \end{pmatrix} \begin{pmatrix} d_{1, \vec{i}, \alpha} \\ d_{2, \vec{i}, \alpha} \end{pmatrix}. \quad (55)$$

The Hund's coupling for antiferromagnetic core spin configuration with wave vector $\vec{K}_{\text{spin}} ((0, 0, \pi)$ for A type AF, (π, π, π) for purely AF) is

$$H_{\text{Hund}} = J_{\text{H}}S_c \sum_{\vec{i}, a} \left[(1 - \exp(i\vec{K}_{\text{spin}} \cdot \vec{i})) d_{i, a, \uparrow}^{\dagger} d_{i, a, \uparrow} + (1 + \exp(i\vec{K}_{\text{spin}} \cdot \vec{i})) d_{i, a, \downarrow}^{\dagger} d_{i, a, \downarrow} \right]. \quad (56)$$

The total Hamiltonian is the sum of the terms considered so far. By diagonalizing this in k space, we can find the energy levels and eigenstates.

Optical conductivity per volume due to the transitions between Mn e_g levels, σ , can be calculated using the eigenstates and energy levels found from the above Hamiltonian. Using the standard linear response theory,^{16,17} optical conductivity is given by

$$\sigma_p^{\lambda\nu} = -\frac{1}{i\omega N_{\text{Mn}} a_0^3} \sum_n \frac{\langle 0 | J_{p\lambda}^{\dagger} | n \rangle \langle n | J_{p\nu} | 0 \rangle}{\hbar\omega - (E_n - E_0) + i\epsilon}, \quad (57)$$

where ϵ is an infinitesimal and J_p is given by $\hat{J}_p = -\frac{iea_0}{2\hbar} \sum_{\vec{i}, \vec{\delta}, a, b, \alpha} t_{\vec{\delta}}^{ab} \vec{\delta} \left(d_{i\alpha}^{\dagger} d_{\vec{i}+\vec{\delta}b\alpha} - H.c. \right)$.¹⁸

V. COMPARISON OF $(\pi, \pi, 0)$ AND (π, π, π) TYPE DISTORTIONS

In the purely local model considered in Ref. 6, for which only nearest-neighbor Mn-O and Mn-Mn springs are considered, we have $K_s = K_{2s}$ and $E_{\text{tot}}^{\text{MIN}}(\pi\pi\pi) = E_{\text{tot}}^{\text{MIN}}(\pi\pi 0)$ up to

order A^2 according to Eqs. (22) and (34). However, in real situation for which farther ion-elastic energies exist, we have $K_s \neq K_{2s}$ and the two distortions have different energies. Equations (22) and (34) shows that if $K_{2s} < K_s$, then the leading order term stabilizes the $(\pi, \pi, 0)$ distortion over the (π, π, π) distortion. If K_s and K_{2s} are very close to K^* , the A^2 term will be smaller for the larger of K_s and K_{2s} , opposite trend of the leading order term. For parameter values determined in Appendix B, we find that $K_{2s} < K_s$ is required to make $(\pi\pi 0)$ distortion favored. Optic phonon spectrum along $\vec{k} = \kappa(\pi, \pi, 0)$ and $\kappa(\pi, \pi, \pi)$ ($0 < \kappa < 1$) would be useful to check this condition. At $\kappa = 0$, these two modes have the same energy. As κ approaches to 1, if the (π, π, π) mode has a higher energy than the $(\pi, \pi, 0)$ mode, it would be an indication that $K_s > K_{2s}$. So far, the phonon spectrum for LaMnO₃ has not been calculated. Ghosez *et al.*¹⁹ have calculated phonon spectra for similar compounds, BaTiO₃, PbTiO₃, and PbZrO₃. These results show that $(\pi, \pi, 0)$ mode (M_2 point in Fig. 1 of Ref. 19) has a higher energy than (π, π, π) mode (R_{12} point in Fig. 1 of Ref. 19) by 11 %, 7%, and 2 % respectively, contrary to our expectation for LaMnO₃. Since the energies of these modes depend sensitively on transition metal elements, a phonon spectrum calculation for LaMnO₃ is necessary.

We examine the possibility that the two distortions have different band energies. For this purpose, we use a tight binding Hamiltonian introduced in the previous section, and calculate the band structures and total band energies for the two distortion patterns. On the first Brillouin zone boundary (i.e., $|k_z| = \pi/2$ or $|k_x| + |k_y| = \pi$ planes) and on the planes satisfying $|k_x| = |k_y|$, we find that the band structures for $(\pi, \pi, 0)$ and (π, π, π) distortions are identical. Between these planes, when a band is well separated from other bands, it has a similar band structure for the $(\pi, \pi, 0)$ and (π, π, π) distortions. Since the filled bands are well separated from the empty bands by the Jahn-Teller splitting, the results show that the change of the filled bands are negligible. We find that the total band energy per Mn ion changes less than 1 meV between the $(\pi, \pi, 0)$ and (π, π, π) distortions. We therefore conclude that the strain (lattice restoring force) effects are crucial.

In our calculation for the strained films, we assume that the sign of the energy difference between the two types of ordering is not changed by applied strains, and consider the $(\pi, \pi, 0)$ ordering only.

VI. RESULTS

A. Lattice and orbital states in strained films

In this section, we present our calculations for strained films. We use $e_{||}$ to denote the substrate induced additional strain, $e_{xx} - e_{xx}^{bulk}$. We examine the strain in the range of $-2\% < e_{||} < 2\%$. Since $a_0 \approx 4.03 \text{ \AA}$, the difference of the xy plane lattice parameter between bulk LaMnO₃ and substrate is between -0.08 \AA and 0.08 \AA . We represent the changes in Q_{3u} , Q_{2s} , and e_{zz} by writing δ in front. For example, $\delta Q_{3u} = Q_{3u} - Q_{3u}^{bulk}$. Our calculation shows that δe_{zz} versus $e_{||}$ in this range is close to linear. We obtain $\delta e_{zz}/e_{||} \approx -1.8$ for the parameter set obtained from Ref. 2, and $\delta e_{zz}/e_{||} \approx -1.4$ for the parameter set obtained from Ref. 20. These ratios are about 2 times larger than the ratio for La_{0.7}Ca_{0.3}MnO₃ film.²⁰ This is due to the softening of the Q_{3u} mode in LaMnO₃.

From δe_{zz} versus e_{\parallel} , we can also find δQ_{1u} and δQ_{3u} versus e_{\parallel} . The results are shown in Fig. 2. To understand these results, we find the leading terms of $\delta Q_{1u}/(a_0 e_{\parallel})$, $\delta Q_{2s}/(a_0 e_{\parallel})$, and $\delta Q_{3u}/(a_0 e_{\parallel})$. They are

$$\frac{\delta Q_{1u}}{a_0 e_{\parallel}} = 2\sqrt{3} \frac{K^* - K_{2s}}{K_B + 2(K^* - K_{2s})} + O(A^2), \quad (58)$$

$$\frac{\delta Q_{2s}}{a_0 e_{\parallel}} = -\frac{3}{\sqrt{2}} \frac{K_B (2K^* - 3K_{2s}) + 4(K^* - K_{2s})^2}{(K_B + 2K^* - 2K_{2s})(K^* - K_{2s})K_{2s}^2} \lambda A + O(A^3), \quad (59)$$

$$\frac{\delta Q_{3u}}{a_0 e_{\parallel}} = -\sqrt{6} \frac{K_B}{K_B + 2(K^* - K_{2s})} + O(A^2). \quad (60)$$

This shows that Q_{2s} changes more slowly than Q_{3u} , because the staggered distortion is coupled to the uniform strain only through the anharmonic term. Since $K^* - K_{2s}$ is almost one order smaller than K_B , Q_{1u} also changes slowly compared with Q_{3u} . Therefore, the main effect of the uniaxial strain is the change in the uniform tetragonal distortion without much change in staggered distortion or volume. Figure 2 shows that $\delta Q_{2s}/(a_0 e_{\parallel})$ can be either positive or negative depending on the parameter values, whereas $\delta Q_{1u}/(a_0 e_{\parallel}) > 0$ and $\delta Q_{3u}/(a_0 e_{\parallel}) < 0$ always.

We obtain $\theta_1 \approx 54.8^\circ$ for the bulk state from Eq. (39). θ_1 versus e_{\parallel} is shown in Fig. 3. The change in θ_1 is about $\pm 5^\circ - 15^\circ$. For tensile strains, θ_1 and θ_2 approach towards 90° , which corresponds to $|x^2 - y^2 \rangle$. For compressive strains, θ_1 and θ_2 approach to 0° and 180° , which corresponds to $|3z^2 - r^2 \rangle$. This can be understood from the fact that in $\theta_1, \theta_2 = |x^2 - y^2 \rangle$ state, the x-y plane Mn-O-Mn distance tends to be farthest, and in $\theta_1, \theta_2 = |3z^2 - r^2 \rangle$, shortest due to the electron distribution in the xy plane.

The change in the Jahn-Teller splitting, $\delta \Delta E_{JT}$, is shown in Fig. 4, which is about ± 0.02 - 0.2 eV for $\pm 2\%$ strain.

B. Magnetic property in strained films

According to Ref. 21, $J_{xy} = -1.66$ meV, $J_z = 1.16$ meV for bulk LaMnO_3 . Since $\theta_1 = 54.8^\circ$ for bulk, we obtain $J_F = 7.52$ meV and $J_{AF} = 4.50$ meV, which corresponds to $J_{xy}^0 = -0.22$ meV, $J_z^0 = 2.62$ meV, and $J^* = 1.88$ meV. Using these parameter values, we find J_{xy} and J_z versus θ_1 , which are plotted in Fig. 5 (a). As the two orbital states approach to $\pi/4$ and $3\pi/4$, i.e., $|z^2 - x^2 \rangle$ and $|z^2 - y^2 \rangle$, both J_{xy} and J_z become more ferromagnetic, and as they approach to 0 and π , i.e., $|3z^2 - r^2 \rangle$ and $|3z^2 - r^2 \rangle$, or to $\pi/2$ and $\pi/2$, i.e., $|x^2 - y^2 \rangle$ and $|x^2 - y^2 \rangle$, J_{xy} and J_z become less ferromagnetic. This is due to the orbital-state-dependent hopping between the filled and empty orbitals, which mediates ferromagnetic interaction. When $20^\circ < \theta_1 < 70^\circ$, the magnetic ground state remains A-type antiferromagnetic. Outside this range, both J_{xy} and J_z become positive, and purely antiferromagnetic state is the ground state. In fact, Fig. 3 shows that 2% tensile strain can change θ_1 close to 70° , and turn the material into a purely antiferromagnetic state.

The mean field estimates of T_c are shown in Fig. 5 (b). T_c for bulk state is about 210 K, somewhat larger than the measured $T_c = 140$ K.²¹ It shows that $\pm 2\%$ strain changes T_c by about ± 50 K. Relatively large change in T_c and the possible change into purely AF

state are due to the strong dependence of magnetism on the e_g orbital state and the strong Jahn-Teller coupling between the e_g orbital state and the lattice distortion.

C. Magnetostriction effects in bulk state

In this subsection we present the magnetostriction effects calculated by the model in Section III. B. We use the two sets of parameter values in Table I and $J^* = 1.88$ meV. The results obtained by numerical minimization of the Landau free energy [Eq. (49)] are shown in Table II. The change in the JT strain, $\delta\epsilon^*$, is about $0.003 \sim 0.01$. $\delta\epsilon^*/[\epsilon^*(T > T_c)]$ is about -0.08 for the parameter set from Ref. 2, and -0.31 for that from Ref. 20. These results show that when the effective JT modulus of Q_{3u} mode, $K^* - K_{2s}$, is smaller, the magnetostriction effect is larger.

We obtain $\alpha \approx 2$, and $2\alpha^2 T_c^0 \approx 0.1$ eV for both parameter sets from Refs. 2 and 20. We obtain $K_\theta = 1.2$ eV for Ref. 2, and $K_\theta = 0.3$ eV for Ref. 20. Therefore, the transition will be of the second order. However, if we have a softer K_θ (a third or a tenth), or a stronger magnetostriction coupling α (twice or three times), then we will have a first-order phase transition. Our numerical minimization of the free energy confirms these results.

Recently, the orbital ordering in LaMnO₃ has been directly observed using a resonant X-ray scattering technique.⁸ In this result, the orbital ordering versus temperature curve has a change of the slope at $T = T_N$. The sign of the change indicates that the orbital states change away from $3x^2 - r^2/3y^2 - r^2$ ($\theta_1 = 60^\circ$) as $T \rightarrow 0$ below T_N , which is consistent with our calculation. Recent neutron diffraction study measured $\sin \theta_1$ versus T .²² Our results predict that $\sin \theta_1$ (which corresponds to c_2 in Fig. 3 in Ref. 22) changes by 0.01 for parameters from Ref. 2 and 0.04 for parameters from Ref. 20 between $T=0$ and $T > T_N$. However, Ref. 22 shows negligible change in $\sin \theta_1$ between $T=0$ and $T > T_N$, which indicates a smaller magnetostriction coupling α , or a larger elastic modulus K_θ than the values obtained above.

D. Band structures in strained films

First, we summarize the band structure in bulk state A-type antiferromagnetic LaMnO₃, which is explained in detail in Ref. 13. Crudely speaking, the bands fall into 4 pairs, which may be understood by setting $t_o = 0$ [as occurs at $\vec{k} = (\pi/2, \pi/2, \pi/2)$]; in this case we have four separate energy levels on each site, which are $E_{1,2} = -\sqrt{\frac{3}{2}}\lambda\sqrt{Q_{2s}^2 + Q_{3u}^2}$, $E_{3,4} = \sqrt{\frac{3}{2}}\lambda\sqrt{Q_{2s}^2 + Q_{3u}^2}$, $E_{5,6} = 2J_H S_c - \sqrt{\frac{3}{2}}\lambda\sqrt{Q_{2s}^2 + Q_{3u}^2}$, and $E_{7,8} = 2J_H S_c + \sqrt{\frac{3}{2}}\lambda\sqrt{Q_{2s}^2 + Q_{3u}^2}$. To find the three parameter values of our model Hamiltonian, i.e., t_0 , λ , and $J_H S_c$, we fit our band structure calculation to the LDA (local density-functional approximation) band calculation for the JT distorted LaMnO₃ in Ref. 14 at high symmetry points in reciprocal space. The standard deviation is ≈ 0.2 eV. The determined parameter values are $t_o = 0.622$ eV, $\lambda = 1.38$ eV/Å, and $2J_H S_c = 2.47$ eV. The fitted band structure is shown in Fig. 1 in Ref. 13.

When the strain does not change A-type antiferromagnetic core spin configuration, the main effect of the strain is the change in the band width. The results are shown in Fig. 6. Solid lines are for the compressive strain, and dashed lines are for the tensile strain. Bulk

band structure can be approximately obtained by taking the average of the two band structures. At $(\pi/2, \pi/2, \pi/2)$, where the effective hopping vanishes, the energy level change is $\delta\Delta E_{JT}$ obtained before. From this point, dispersions along $(\pi/2, \pi/2, 0)$ and along $(\pi, 0, \pi/2)$ represent the hoppings in z direction and in xy plane, respectively. Between $(\pi/2, \pi/2, \pi/2)$ and $(\pi/2, \pi/2, 0)$, the widths of the lower JT bands, $E_{1,2}$ and $E_{5,6}$, are increased for compressive strains, whereas the widths of the upper JT bands, $E_{3,4}$ and $E_{7,8}$, are decreased. This is related to the changes in θ_1 and θ_2 due to the strains: As θ_1 and θ_2 approach to 0 and π , the lower JT level approaches to $3z^2 - r^2$ state which has a large hopping along z direction, whereas the upper JT level approaches to $x^2 - y^2$ which has no hopping along z direction. But between $(\pi/2, \pi/2, \pi/2)$ and $(\pi, 0, \pi/2)$, the dispersion does not change much, indicating that the average hopping is not changed much in xy plane due to the alternating orbital pattern in xy plane.

As pointed out in the previous section, 2 % tensile strain may induce purely antiferromagnetic ground state. Due to the strong Hund's coupling, this results in substantial changes in band structure and optical conductivity as shown below and in the next section, respectively. Band structure for the purely AF state can be obtained by using $\vec{K}_{spin} = (\pi, \pi, \pi)$ in the model described in Sect. IV. The results are shown in Fig. 7 for the same lattice distortions and parameters used for the band structure shown as dotted lines in Fig. 6. Between $(\pi/2, \pi/2, \pi/2)$ and $(\pi/2, \pi/2, 0)$, the two band structures are identical since it involves only z direction hopping. Between $(\pi/2, \pi/2, \pi/2)$ and $(\pi, 0, \pi/2)$, where only xy directional hopping is involved, for A-type AF state the different JT levels repel each other, while for purely AF state the different Hund's levels repel each other. This represents different mixings for different spin configurations: the mixing for A-type AF state is mainly between the different JT states, while the mixing for purely AF state is mainly between the different Hund's states. The band structure between $(\pi, 0, 0) - (0, 0, 0) - (\pi/2, \pi/2, \pi/2)$ shows the same trend, which results in a small indirect band gap for the purely AF state. However, due to the on-site Coulomb repulsion of about 1-2 eV neglected in the above calculation¹³ it is unlikely to have the insulator-to-semimetal transition in this material.

E. Optical conductivities in strained films

From the band structure, we have calculated optical conductivities for strained films in A-type AF ground state. Results are shown in Fig. 8. σ_{xx} or σ_{yy} (solid lines) shows a relatively small changes by strains. The spectral weight of the Hund's peak in σ_{zz} (dotted lines) at around 2.5 eV is increased (decreased) about 20 % as we apply 2 % compressive (tensile) strain. This seems consistent with the change of the average hopping along z direction by strains mentioned in the previous section.

Optical conductivities for the purely AF state are calculated in the same way. Figure 9 shows the results for σ_{xx} (solid line) and σ_{zz} (dotted line). First, the sharp Hund's peak in σ_{zz} is disappeared. This can be understood from the band structure, particularly between $(\pi/2, \pi/2, \pi/2)$ and $(\pi, 0, \pi/2)$. The sharp Hund's peak in σ_{zz} for A-type AF state originates from the two parallel bands split by the Hund's coupling, $2J_H S_c$. However, this structure disappears when we have purely AF core spin as seen in Fig. 7. Comparison of Fig. 9 (a) (2 % strain) and (b) (bulk) shows that as orbital state is changed toward $x^2 - y^2$ by the tensile

strain, which has zero hopping along z-direction, the spectral weight of the Hund's peak in σ_{zz} decreases, as observed for the A-type AF state in Fig. 8. σ_{xx} shows prominent peaks at the Hund's splitting (2.5-3.5 eV) and at the Hund-plus-JT splitting (4-5 eV) due to purely AF spin state in contrast to the A-type AF state (see Fig. 8). The JT peaks at around 1 eV in both σ_{xx} and σ_{zz} are due to the strong hybridization between major and minor spin states. If we increase $J_H S_c$ and reduce this hybridization, the JT peaks decrease, as can be seen by comparing Figs. 9(a) and 9(c). Above results show that changes in xy plane spin configuration make differences in σ_{zz} due to the changes in hybridization.

For the calculations so far, we have assumed zero on-site Coulomb repulsion U . However, as explained in Ref. 13, in this material there exists $U \approx 1.6$ eV. Therefore actual peak positions will be higher by ~ 1.6 eV and the spectral weight of each peak will be reduced inversely proportional to the peak energy.

VII. CONCLUSION

In summary, we developed a model of elastic energy for LaMnO_3 and solved for uniaxial strains in thin films. We found that $\pm 2\%$ strain can change the uniform tetragonal strain and e_g orbital states without much change in the staggered distortion or volume. We found that 2% tensile strain can change the magnetic ground state into purely antiferromagnetic state, inducing dramatic changes in band structure and optical conductivity. Magnetostriction effect at T_N in bulk state is found to be large. We examined the possibility that the lattice energy will favor $(\pi\pi 0)$ ordering over $(\pi\pi\pi)$ ordering. We also noted “ Q_{3u} mode softening” in LaMnO_3 . The results presented in this paper for LaMnO_3 show the strong coupling between lattice, Mn e_g orbital state, and exchange interaction, which lies at the root of the novel properties of doped manganese perovskites.

This work is supported by NSF-DMR-9705182 and the University of Maryland MRSEC.

APPENDIX A: GENERAL EXPRESSION OF ELASTIC ENERGY FOR STAGGERED DISTORTION

In this Appendix, we show how we can get the general expression of the elastic energy due to distortions with wave vector \vec{k} in perovskite structure. We again consider three dimensional displacement of Mn ion, $\vec{\delta}$, and the displacements of oxygen ions along Mn-Mn axis, u^x , u^y , and u^z as defined in the text and shown in Fig. 1. We consider the displacements with wave vector \vec{k} , $\vec{\delta}_i = \vec{\delta}_k e^{i\vec{k}\cdot\vec{i}}$ and $u_i^{x,y,z} = u_k^{x,y,z} e^{i\vec{k}\cdot\vec{i}}$. When we define $d_{1,2,3}(\vec{k}) = \delta_k^{x,y,z}$ and $d_{4,5,6}(\vec{k}) = u_k^{x,y,z}$, the energy due to these strains, $E_s(\vec{k})$, is given by

$$E_s(\vec{k}) = \sum_{i,j} d_i(\vec{k}) D_{ij}(\vec{k}) d_j(\vec{k}), \quad (\text{A1})$$

where $D_{ij}(\vec{k}) = D_{ji}(\vec{k})$.

In special cases, symmetry arguments make certain terms vanish or equal. First, when $k_x = \pi$, mirror symmetry operation about $x = 0$ plane changes k_x to $-k_x$. Since $k_x = \pi$ and $k'_x = -\pi$ are equivalent, the symmetry operation changes \vec{k} back to \vec{k} . Since this

operation changes δ_k^x to $-\delta_k^x$, odd order terms of δ_k^x should vanish, and therefore, $D_{12}(\vec{k}) = D_{13}(\vec{k}) = D_{14}(\vec{k}) = D_{15}(\vec{k}) = D_{16}(\vec{k}) = 0$. Second, when $k_x = 0$, mirror symmetry operation about $x = 0$ plane changes \vec{k} back to \vec{k} , δ_k^x to $-\delta_k^x$, and u_k^x to $-u_k^x$. Therefore, odd order terms of δ_k^x and u_k^x vanish. Therefore, $D_{12}(\vec{k}) = D_{13}(\vec{k}) = D_{15}(\vec{k}) = D_{16}(\vec{k}) = 0$ and $D_{42}(\vec{k}) = D_{43}(\vec{k}) = D_{45}(\vec{k}) = D_{46}(\vec{k}) = 0$. Third, when $k_x = \pm k_y$, mirror operation interchanging x axis and $\pm y$ axis changes \vec{k} back to \vec{k} , and δ_x to $\pm\delta_y$, u_x to $\pm u_y$. Therefore, $D_{11}(\vec{k}) = D_{22}(\vec{k})$, $D_{44}(\vec{k}) = D_{55}(\vec{k})$, $D_{14}(\vec{k}) = D_{25}(\vec{k})$, $D_{15}(\vec{k}) = D_{24}(\vec{k})$, $D_{1j}(\vec{k}) = \pm D_{2j}(\vec{k})$, $D_{4j}(\vec{k}) = \pm D_{5j}(\vec{k})$, where $j = 3, 6$

If we apply these rules to $\vec{k} = (\pi, \pi, 0)$, and (π, π, π) distortions, we obtain the following expressions.

$$\begin{aligned} \frac{E_s[\vec{k} = (\pi, \pi, 0)]}{N_{Mn}} &= D_{11}(\vec{k})(\delta_k^{x2} + \delta_k^{y2}) + D_{33}(\vec{k})\delta_k^{z2} + D_{44}(\vec{k})(u_k^{x2} + u_k^{y2}) \\ &\quad + D_{66}(\vec{k})u_k^{z2} + 2D_{45}(\vec{k})u_k^x u_k^y + 2D_{36}(\vec{k})\delta_k^z u_k^z. \end{aligned} \quad (\text{A2})$$

$$\begin{aligned} \frac{E_s[\vec{k} = (\pi, \pi, \pi)]}{N_{Mn}} &= D_{11}(\vec{k})(\delta_k^{x2} + \delta_k^{y2} + \delta_k^{z2}) + D_{44}(\vec{k})(u_k^{x2} + u_k^{y2} + u_k^{z2}) \\ &\quad + 2D_{45}(\vec{k})(u_k^x u_k^y + u_k^y u_k^z + u_k^z u_k^x). \end{aligned} \quad (\text{A3})$$

K_{2s} , K_{3s} , and K_s in the text are defined as $K_{2s} = [D_{44}(\pi\pi 0) - D_{45}(\pi\pi 0)]/2$, $K_{3s} = 3[D_{44}(\pi\pi 0) + D_{45}(\pi\pi 0)]/2$, and $K_s = [D_{44}(\pi\pi\pi) - D_{45}(\pi\pi\pi)]/2$. Therefore, the condition for $K_{3s} > K_{2s}$ is $D_{44}(\pi\pi 0) > -2D_{45}(\pi\pi 0)$. We expect this condition is well-satisfied for the following reasons: First, the stability of lattice implies $D_{44}(\pi\pi 0) > 0$. Second, the Coulomb repulsion between oxygen will favor similar O-O distances, which implies $D_{45}(\pi\pi 0) > 0$.

APPENDIX B: PARAMETERS FOR THE MODEL OF ELASTIC ENERGY

Optical absorption experiment for LaMnO₃ shows Mn-O bond stretching mode peak at 70.3 meV.²³ From this we can find the effective Mn-O spring constant $K_1 = 7.36 \text{ eV/\AA}^2$ (Ref. 13). If we assume that K_1 is the main contribution to K_{2s} , we obtain $K_{2s} \approx K_1/2 = 3.68 \text{ eV/\AA}^2$. In Ref. 13, we used this value of K_1 to estimate the Jahn-Teller coupling constant λ , the value of which is consistent with LDA band calculation.¹³

For La_{0.83}Sr_{0.17}MnO₃, c_{11} and c_{12} have been measured in an ultrasound experiment.²⁴ We believe the bulk modulus $c_B = (c_{11} + 2c_{12})/3 = 143 \text{ GPa}$ ($K_B = 10.8 \text{ eV/\AA}^2$) of La_{0.83}Sr_{0.17}MnO₃ at 200 K (orthorhombic structure) can be used as an approximate value for the bulk modulus of LaMnO₃. The value of c_B at 310 K (rhombohedral phase) is about 176 GPa, which gives a rough estimate of uncertainty in c_B of about 20 %.

Since La_{0.83}Sr_{0.17}MnO₃ is in the doping region where a structural change happens,²⁵ and c^* is sensitive to the structural transition unlike bulk modulus, we do not believe the measured c^* of this material is a good estimate of c^* for LaMnO₃. Indeed, c^* for La_{0.83}Sr_{0.17}MnO₃

is much smaller than those for other typical perovskite oxides.²⁶ For example, the LDA calculation in Ref. 26 predicted $c_B = 199$ GPa, $c^* = 142$ GPa, and $c^*/c_B = 0.71$ for SrTiO₃, which is close to the measurements for SrTiO₃, $c_B = 179$ GPa, $c^* = 115$ GPa, and $c^*/c_B = 0.64$. The same LDA calculation results showed that other perovskite oxides, such as BaTiO₃, CaTiO₃, KNbO₃, NaNbO₃, PbTiO₃, PbZrO₃, BaZrO₃. However, for La_{0.83}Sr_{0.17}MnO₃, $c_B = 143$ GPa, $c^* = 48$ GPa, and $c^*/c_B = 0.34$ at 200 K and $c_B = 176$ GPa, $c^* = 35$ GPa, and $c^*/c_B = 0.20$ at 300 K. Therefore c^*/c_B ratio is less than half of the values for typical perovskites.

Therefore, we instead use the c_{12}/c_{11} ratio measured in La_{0.7}Ca_{0.3}MnO₃ thin film (Ref. 2) and La_{0.6}Sr_{0.4}MnO₃ thin film (Ref. 20), since their doping ranges are relatively far from the structural phase transition doping ratios. The results are $c_{12}/c_{11} = 0.312$ for Ref. 2 and $c_{12}/c_{11} = 0.374$ for Ref. 20. Using

$$\frac{c^*}{c_B} = \frac{3}{2} \frac{1 - c_{12}/c_{11}}{1 + 2c_{12}/c_{11}}, \quad (\text{B1})$$

we obtain c^* and K^* shown in Table I.

We obtain Q_{2s}^{eq} and Q_{3u}^{eq} for bulk LaMnO₃ from crystallography data: $Q_{2s}^{eq} = 0.398 \text{ \AA}$, $Q_{3u}^{eq} = -0.142 \text{ \AA}$ (Ref. 4). Therefore, the three unknown quantities of the model, Q_{1u}^{eq} , λ , and A , are determined from the equilibrium condition:

$$\left. \frac{\partial E}{\partial Q_{1u}} \right|_{eq} = 0, \quad \left. \frac{\partial E}{\partial Q_{2s}} \right|_{eq} = 0, \quad \left. \frac{\partial E}{\partial Q_{3u}} \right|_{eq} = 0. \quad (\text{B2})$$

Obtained parameter values are shown in Table I. The values of A are small enough to justify our approximation of anharmonic terms. For example, the largest dropped term, $AQ_{3u}^3/(3\sqrt{2})$, is 0.5-2 % of $K^*Q_{3u}^2/2$ for parameters in Table I. We obtain $Q_{1u}^{eq} = 0.024 \text{ \AA}$ and 0.005 \AA for the parameters from Refs. 2 and 20, respectively, which shows that the average bond length does not change much. Therefore, it is reasonable to approximate a_0 by the average Mn-Mn distance observed in bulk LaMnO₃, 4.03 \AA . The λ values are close to the independent estimate $\lambda = 1.38 \text{ eV/\AA}$ obtained from band structure fitting. Negative sign of A is consistent with thermal expansion. It is noteworthy that the size of A is largely different for the two parameter sets, which is the consequence of the Q_{3u} mode softening: a small difference in K^* gives a quite large difference in $K^* - K_{2s}^2$ (0.89 eV/\AA^2 and 0.19 eV/\AA^2 for the parameters from Refs. 2 and 20, respectively), which results in a large difference in the estimate of A .

REFERENCES

- * On leave from Department of Physics and Astronomy, The Johns Hopkins University, Baltimore, Maryland 21218.
- ¹ see, e.g. the articles in *Philos. Trans. R. Soc. London, Ser. A*, **356**, No. 1752, pp. 1469-1712 (1998).
- ² A. J. Millis, A. Goyal, M. Rajaewari, K. Ghosh, R. Shreekala, R. L. Greene, R. Ramesh, and T. Venkatesan (to be published).
- ³ B. S. Teo, N. D. Mathur, S. P. Issac, J. E. Evetts, and M. G. Blanière, *J. Appl. Phys.* **83**, 7157 (1998); J. Z. Sun, D. W. Abraham, R. A. Rao, and C. B. Eom, *Appl. Phys. Lett.* **74**, 3017 (1999); R. A. Rao, D. Lavric, T. K. Nath, C. B. Eom, L. Wu, and F. Tsui, *Appl. Phys. Lett.* **73**, 3294 (1999); J. O'Donnell, M. Onellion, M. S. Rzechowski, J. N. Eckstein, and I. Bozovic, *Phys. Rev. B* **54**, 6841 (1996); Y. Suzuki, H. Y. Hwang, S-W. Cheong, and R. B. van Dover, *Appl. Phys. Lett.* **71**, 140 (1997); K. A. Thomas, P. S. I. P. N. de Silva, L. F. Cohen, A. Hossain, M. Rajeswari, T. Venkatesan, R. Hiskes, J. L. MacManus-Driscoll, *J. Appl. Phys.* **84**, 3939 (1998); W. Prellier, A. Biswas, M. Rajeswari, T. Venkatesan, and R. L. Greene, *Appl. Phys. Lett.* **75**, 397 (1999); H. S. Wang, Q. Li, K. Liu, and C. L. Chien, *Appl. Phys. Lett.* **74**, 2212 (1999).
- ⁴ J. B. A. A. Ellemans, B. van Laar, K. R. van der Veen, and B. O. Loopstra, *J. Solid State Chem.* **3**, 238 (1971).
- ⁵ J. Kanamori, *J. Appl. Phys.* **31**, 14S (1960).
- ⁶ A. J. Millis, *Phys. Rev. B* **53**, 8434 (1996).
- ⁷ A. J. Millis, *Phys. Rev. B* **55**, 6405 (1997).
- ⁸ Y. Murakami, J. P. Hill, D. Gibbs, M. Blume, I. Koyama, M. Tanaka, H. Kawata, T. Arima, Y. Tokura, K. Hirota, and Y. Endoh, *Phys. Rev. Lett.* **81**, 582 (1998).
- ⁹ This expression can be written in more symmetric way. For the staggered distortion with wave vector $\vec{\kappa}$,
- $$E_s(\vec{\kappa}) = \frac{1}{2} \tilde{Q}^T (K_{av}I + \Delta\vec{K}_{\vec{\kappa}} \cdot \vec{\tau}) \tilde{Q},$$
- where $\tilde{Q}^T = (Q_{2s}, Q_{3s})$, I is a unit matrix, $\vec{\tau} = \sigma_x \hat{x} + \sigma_z \hat{z}$, σ_x and σ_z are Pauli matrix, $\Delta\vec{K}_{(\pi\pi\pi)} = 0$. For $\vec{\kappa} = (\pi\pi 0)$, $(0\pi\pi)$, and $(\pi 0\pi)$, $\Delta\vec{K}_{\vec{\kappa}} = \Delta K(\sin \psi_{\vec{\kappa}} \hat{x} + \cos \psi_{\vec{\kappa}} \hat{z})$, where $\psi_{(\pi\pi 0)} = 0$, $\psi_{(0\pi\pi)} = 2\pi/3$, $\psi_{(\pi 0\pi)} = -2\pi/3$.
- ¹⁰ In our calculation, we will only consider square substrate lattice, which will not generate any Q_{2u} strain. Therefore, we only need this term for the current study. If we want to find the strain effect for non-square substrate, we should include the terms with Q_{2u} also.
- ¹¹ O. N. Mryasov, R. F. Sabiryanov, A. J. Freeman, and S. S. Jaswal, *Phys. Rev. B* **56**, 7255 (1997); I. Solovyev, N. Hamada, and K. Terakura, *Phys. Rev. Lett.* **76**, 4825 (1996).
- ¹² N. W. Ashcroft, and N. D. Mermin, *Solid State Physics* (Saunders College Publishing, Fort Worth, TX, 1976).
- ¹³ K. H. Ahn and A. J. Millis, *Phys. Rev. B* (to be published, cond-mat/9901127).
- ¹⁴ S. Satpathy, Z. S. Popovic, and F. R. Vukajlovic, *J. Appl. Phys.* **79**, 4555 (1996).
- ¹⁵ S. Satpathy, Z. S. Popovic, and F. R. Vukajlovic, *Phys. Rev. Lett.* **76**, 960 (1996); W. E. Pickett and D. J. Singh, *Phys. Rev. B* **53**, 1146 (1996).

- ¹⁶ A. J. Millis and S. Coppersmith, Phys. Rev. B. **42**, 10807 (1990).
- ¹⁷ E. Dagotto, Rev. Mod. Phys. **66** 763 (1994).
- ¹⁸ The Drude part is zero, because we deal with insulators only.
- ¹⁹ Ph. Ghosez, E. Cockayne, U. V. Waghmare, and K. M. Rabe, Phys. Rev. B. **60**, 836 (1999).
- ²⁰ M. Kawasaki, M. Izumi, Y. Konishi, T. Manako, and Y. Tokura, Mater. Sci. Eng. B **63**, 49 (1999) .
- ²¹ F. Moussa, H. Hennion, J. Rodriguez-Carvajal, and H. Moudden, Phys. Rev. B **54**, 15149 (1996).
- ²² J. Rodriguez-Carvajal, M. Hennion, F. Moussa, A. H. Moudden, L. Pinsard, and A. Revcolevschi, Phys. Rev. B. **57**, 3189 (1998).
- ²³ J. H. Jung, T. W. Noh (private communication).
- ²⁴ T. W. Darling, A. Migliori, E. G. Moshopoulou, S. A. Trugman, J. J. Neumeier, J. L. Sarrao, A. R. Bishop, Phys. Rev. B. **57**, 5093 (1998).
- ²⁵ A. Urushibara, Y. Moritomo, T. Arima, A. Asamitsu, G. Kido, and Y. Tokura, Phys. Rev. B. **51**, 14103 (1995).
- ²⁶ R. D. King-Smith and D. Vanderbilt, Phys. Rev. B, **49**, 5836 (1994).

FIGURES

FIG. 1. Degrees of freedom considered in our model, $\vec{\delta}_i$ and $u_i^{x,y,z}$.

FIG. 2. δQ_{1u} , δQ_{2s} , δQ_{3u} versus $e_{||}$ for (a) $K_B=10.8 \text{ eV/\AA}^2$, $K^*=3.87 \text{ eV/\AA}^2$, $\lambda=1.25 \text{ eV/\AA}$, $K_{2s}=3.68 \text{ eV/\AA}^2$, $A=-0.329 \text{ eV/\AA}^3$, which are the parameter values from Ref. 2, and (b) $K_B=10.8 \text{ eV/\AA}^2$, $K^*=4.57 \text{ eV/\AA}^2$, $\lambda=1.13 \text{ eV/\AA}$, $K_{2s}=3.68 \text{ eV/\AA}^2$, $A=-1.65 \text{ eV/\AA}^3$, which are parameter values from Ref. 20, shown in Table I.

FIG. 3. θ_1 versus $e_{||}$: The solid line is for the parameter values from Ref. 2, and the dashed line is for the parameter values from Ref. 20, shown in Table I.

FIG. 4. δE_{JT} versus $e_{||}$. Solid line is for the parameter values from Ref. 2, and dashed line is for the parameter values from Ref. 20, shown in Table I.

FIG. 5. (a) Magnetic coupling constant J_{xy} (solid line) and J_z (dotted line) versus orbital state θ_1 . (b) Mean field estimation of T_c versus orbital state θ_1 . the ground state is A type antiferromagnetic between 20° and 70° , and purely antiferromagnetic outside this range.

FIG. 6. Band structures for 2 % compressive strain (solid lines) and 2 % tensile strain (dotted lines) for the parameter values from Ref. 2, shown in Table I. Tight binding model parameter values are $t_0=0.622 \text{ eV}$, $2J_H S_c=2.47 \text{ eV}$, and $\lambda=1.13 \text{ eV}$. A-type antiferromagnetic ground state is assumed.

FIG. 7. Band structure for purely antiferromagnetic core spin state for 2 % strain for the parameter values from Ref. 2 shown in Table I, to be compared with the dotted lines in Fig. 6. The tight binding parameter values are $t_0=0.622 \text{ eV}$, $2J_H S_c=2.47 \text{ eV}$, and $\lambda=1.13 \text{ eV}$.

FIG. 8. Optical conductivities, σ_{xx} (solid lines) and σ_{zz} (dotted lines), for 2 % compressive strain (top panels), bulk (middle panels), and 2 % tensile strain (bottom panels) for the parameter values from Ref. 2 (left panels) and for the parameter values from Ref. 20 (right panels) shown in Table I. A-type antiferromagnetic core spin state is assumed.

FIG. 9. Optical conductivities, σ_{xx} (solid lines) and σ_{zz} (dotted lines), for purely antiferromagnetic core spin configuration with (a) 2 % tensile strain, (b) bulk, and (c) a larger Hund coupling and 2 % tensile strain. Lattice distortions in Fig. 1 (a), $t_0=0.622 \text{ eV}$, $2J_H S_c=2.47 \text{ eV}$, and $\lambda=1.13 \text{ eV}$ are used for the calculation.

TABLES

TABLE I. Obtained values of parameters: c_B and K_B are from Ref. 24, and K_{2s} is from the optic phonon mode frequency. We use two experimental results in Refs. 2 and 20 to obtain the two sets of parameters shown here. Details about how these numbers are obtained are shown in Appendix B.

Source	c_B (GPa)	c^* (GPa)	K_B (eV/Å ²)	K^* (eV/Å ²)	K_{2s} (eV/Å ²)	λ (eV/Å)	A (eV/Å ³)	$K^* - K_{2s}$ (eV/Å ²)
Ref. 2	143	90.8	10.8	4.57	3.68	1.13	-1.65	0.89
Ref. 20	143	76.8	10.8	3.87	3.68	1.13	-0.329	0.19

TABLE II. Magnetostriction effect (numerical calculation)

T	parameters	Q_{1u} (Å)	Q_{2s} (Å)	Q_{3u} (Å)	θ_1	ϵ^*
T=0	from Ref. 2	0.0246	0.401	-0.131	53.6°	-0.0328
	from Ref. 20	0.0051	0.411	-0.099	51.5°	-0.0248
$T > T_c$	from Ref. 2	0.0244	0.399	-0.142	54.8°	-0.0355
	from Ref. 20	0.0049	0.399	-0.143	54.8°	-0.0358
Differences between $T = 0$ and $T > T_c$	from Ref. 2	2.5×10^{-4}	0.0024	0.011	-1.2°	0.0028
	from Ref. 20	2.6×10^{-4}	0.012	0.044	-3.4°	0.011

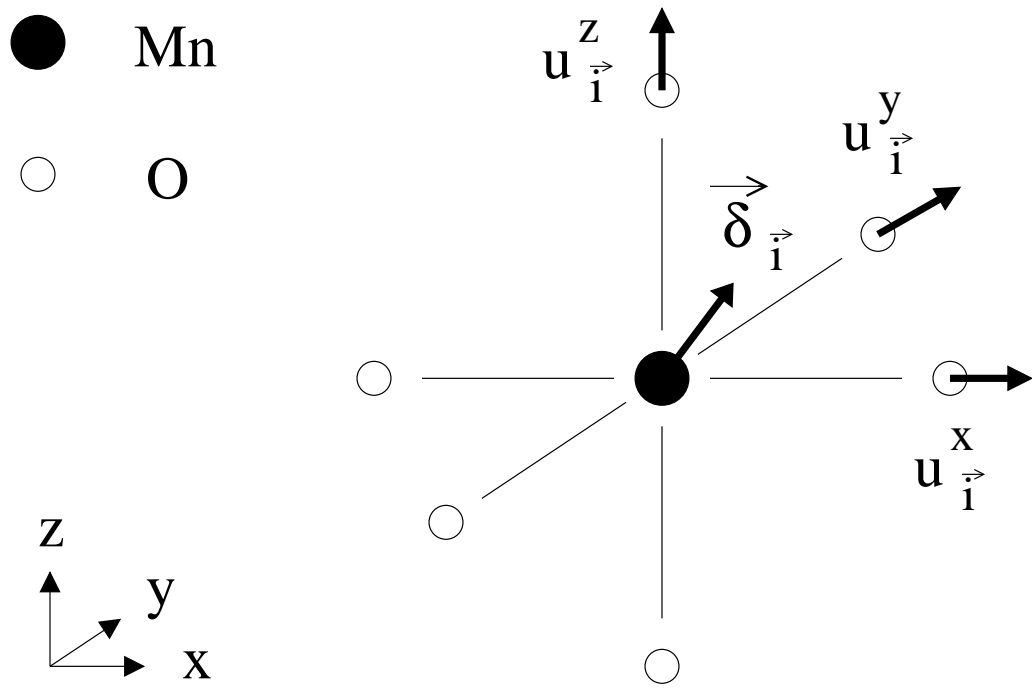


Fig. 1, Ahn and Millis

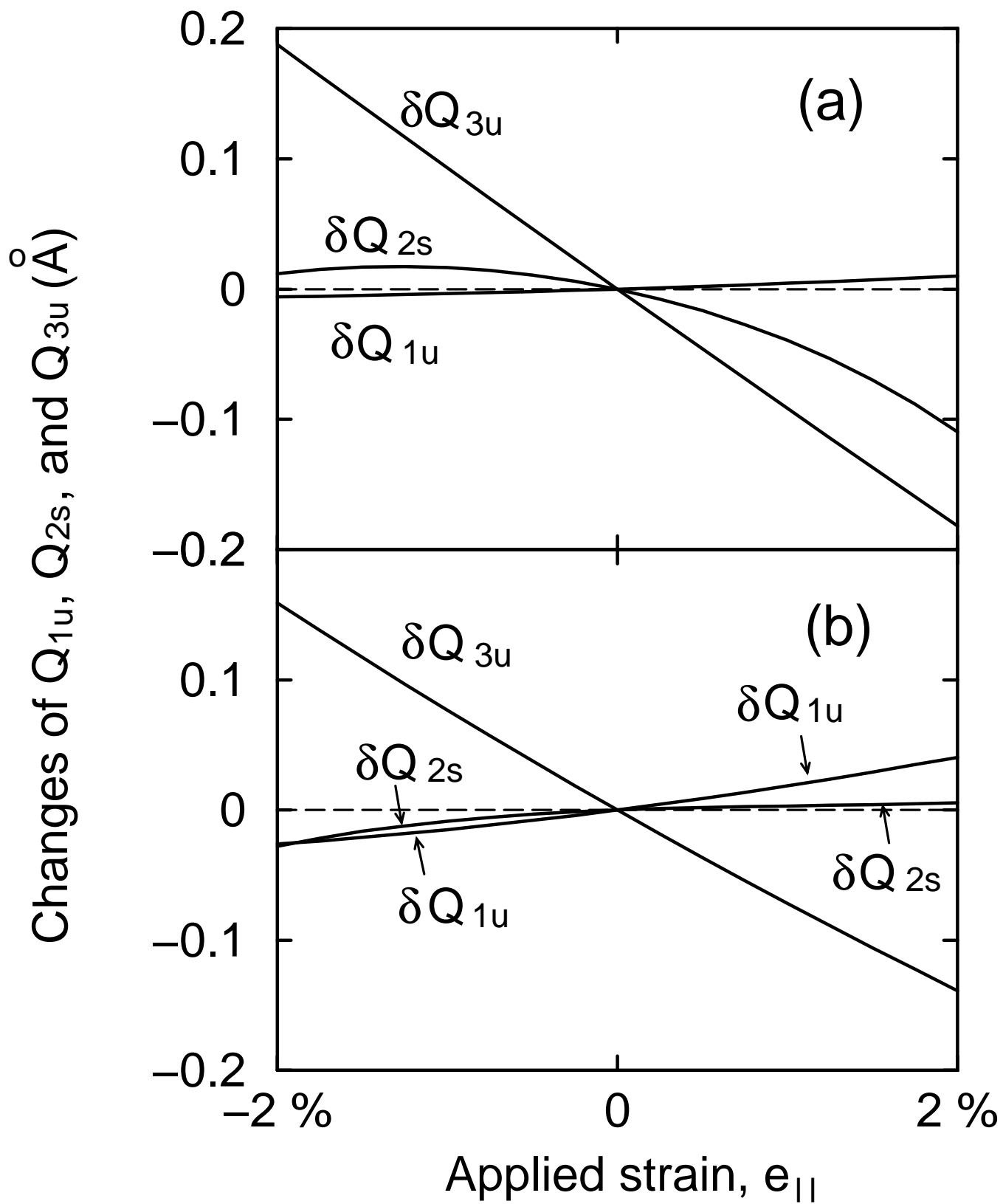


Fig. 2, Ahn and Millis

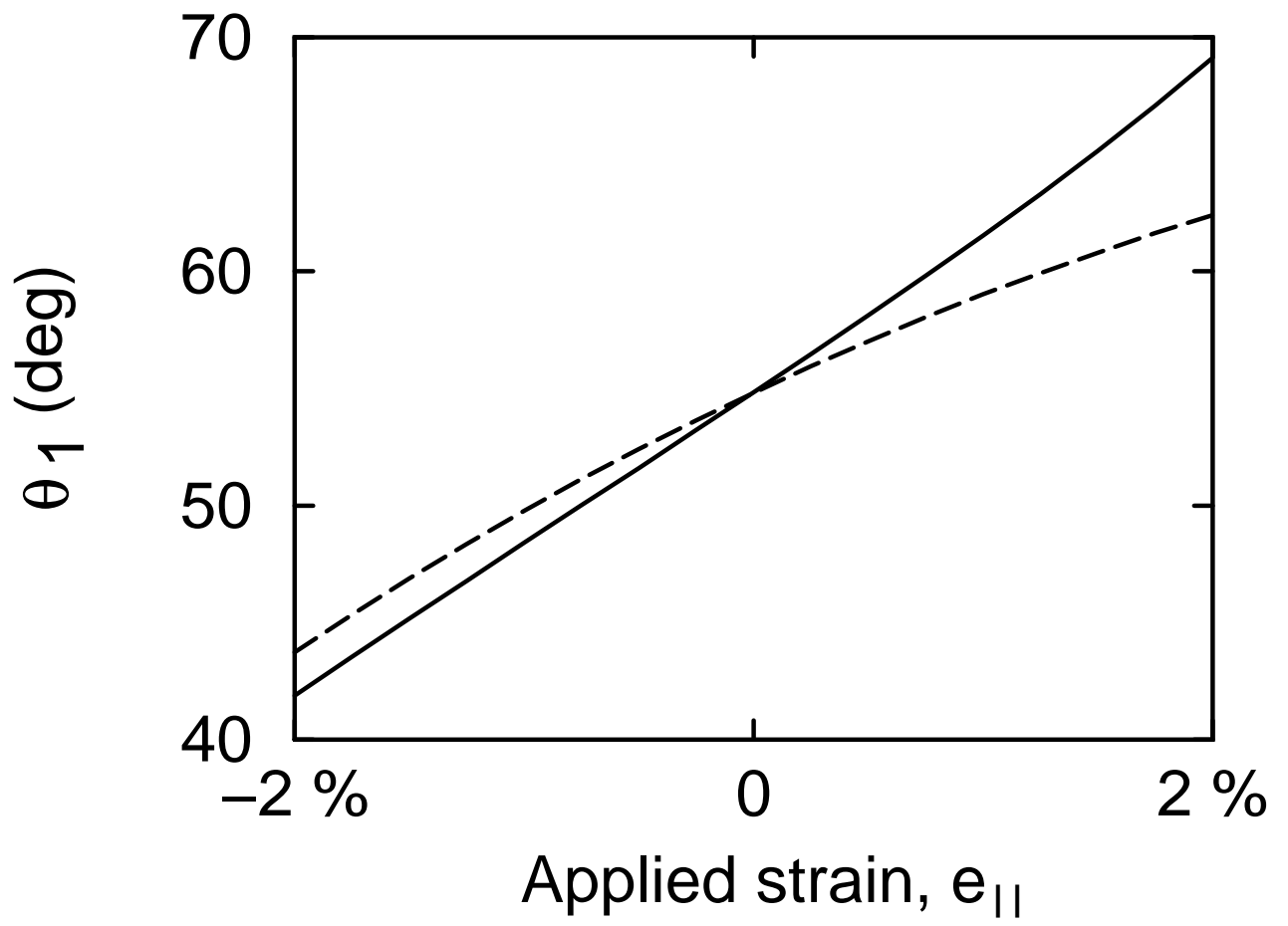


Fig. 3, Ahn and Millis

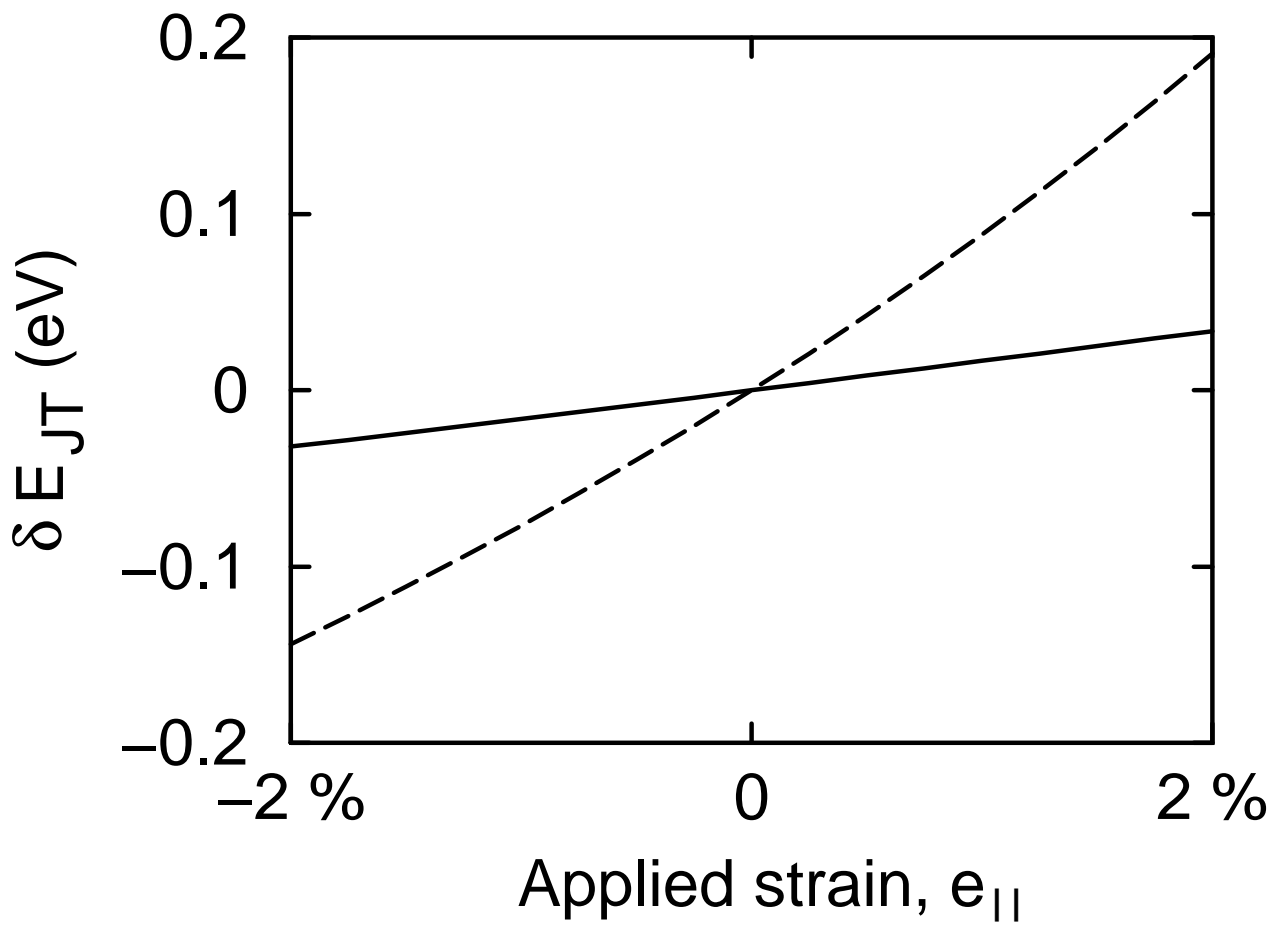


Fig. 4, Ahn and Millis

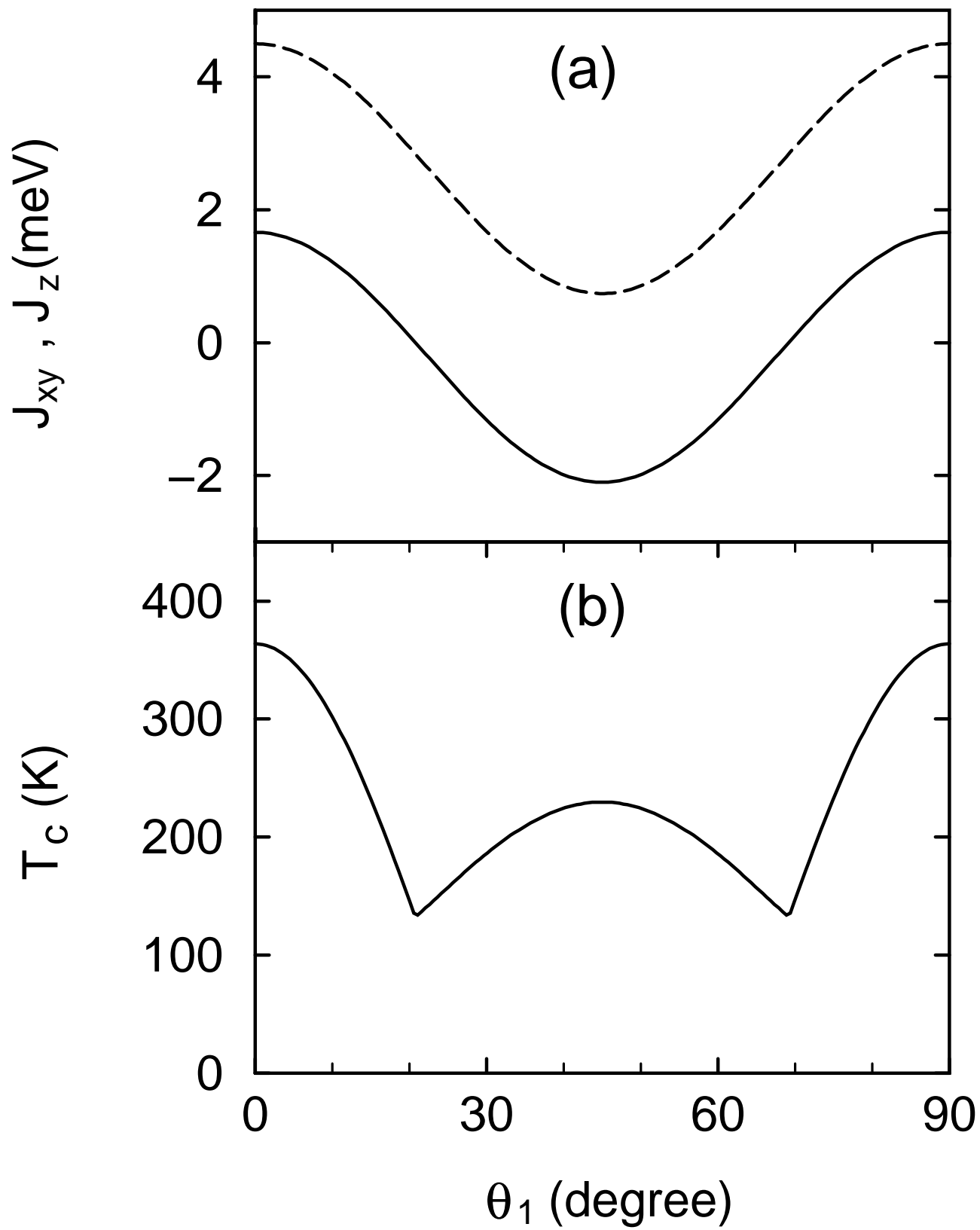


Fig. 5, Ahn and Millis

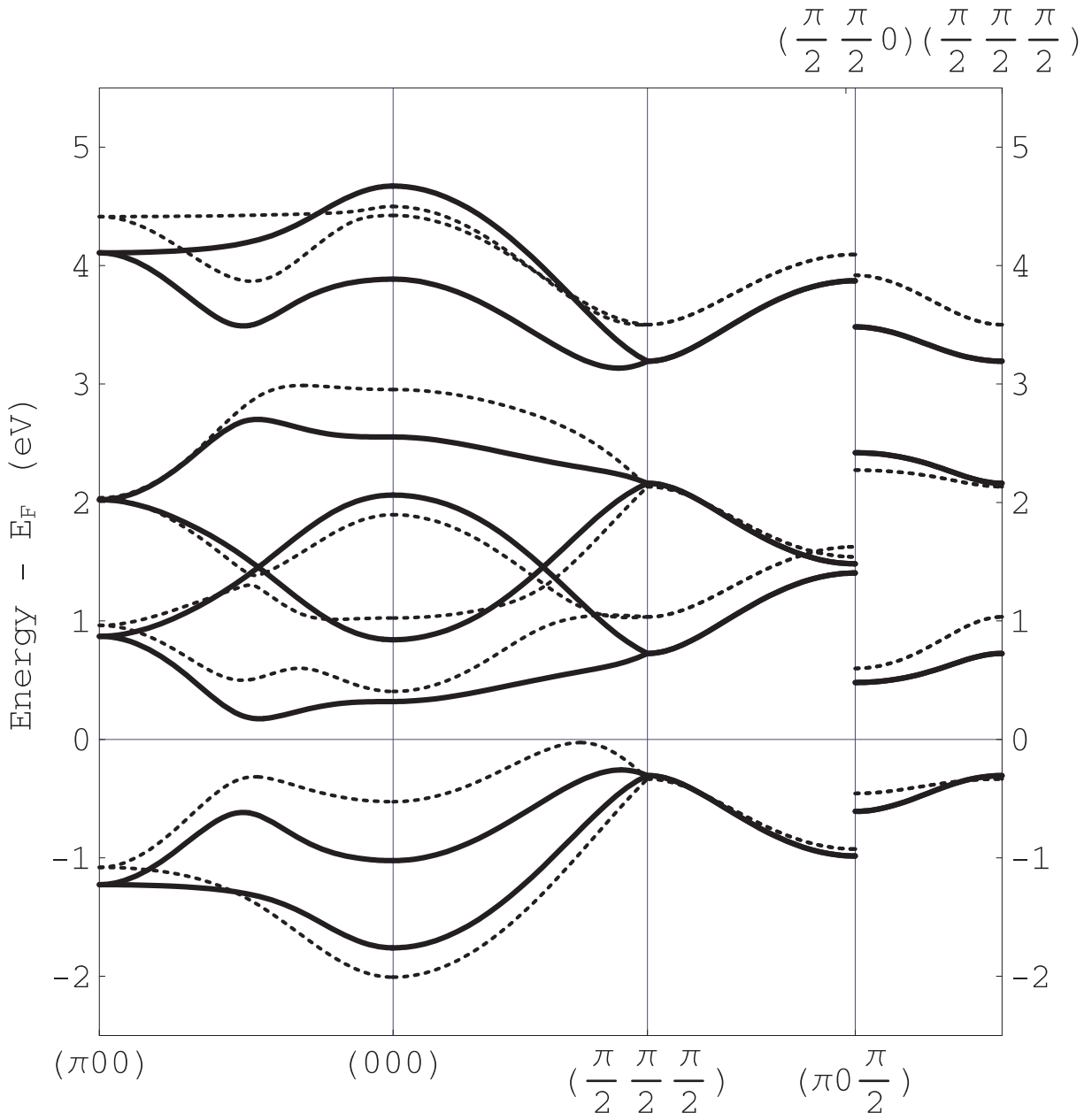


Fig. 6, Ahn and Millis

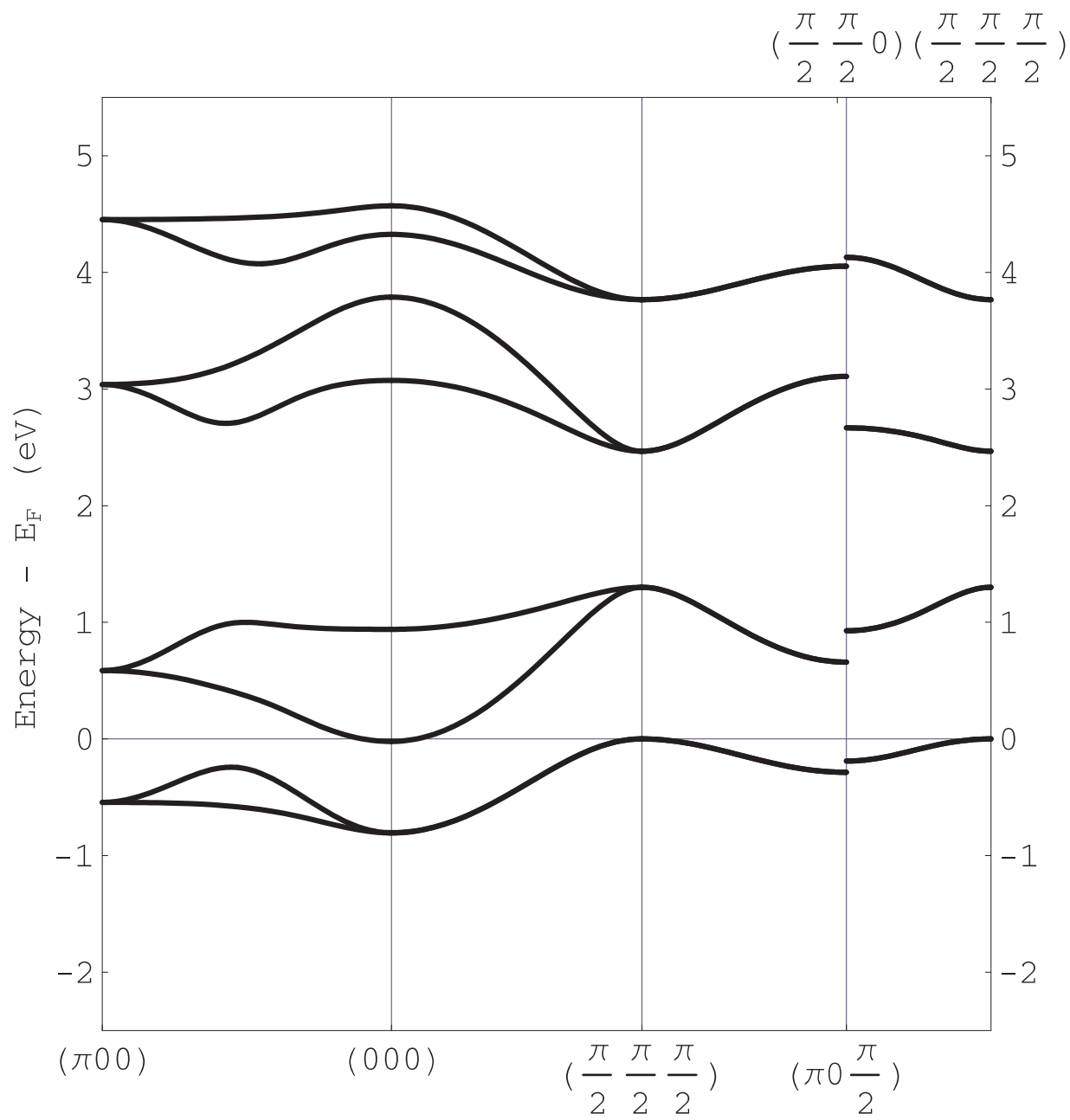


Fig. 7, Ahn and Millis

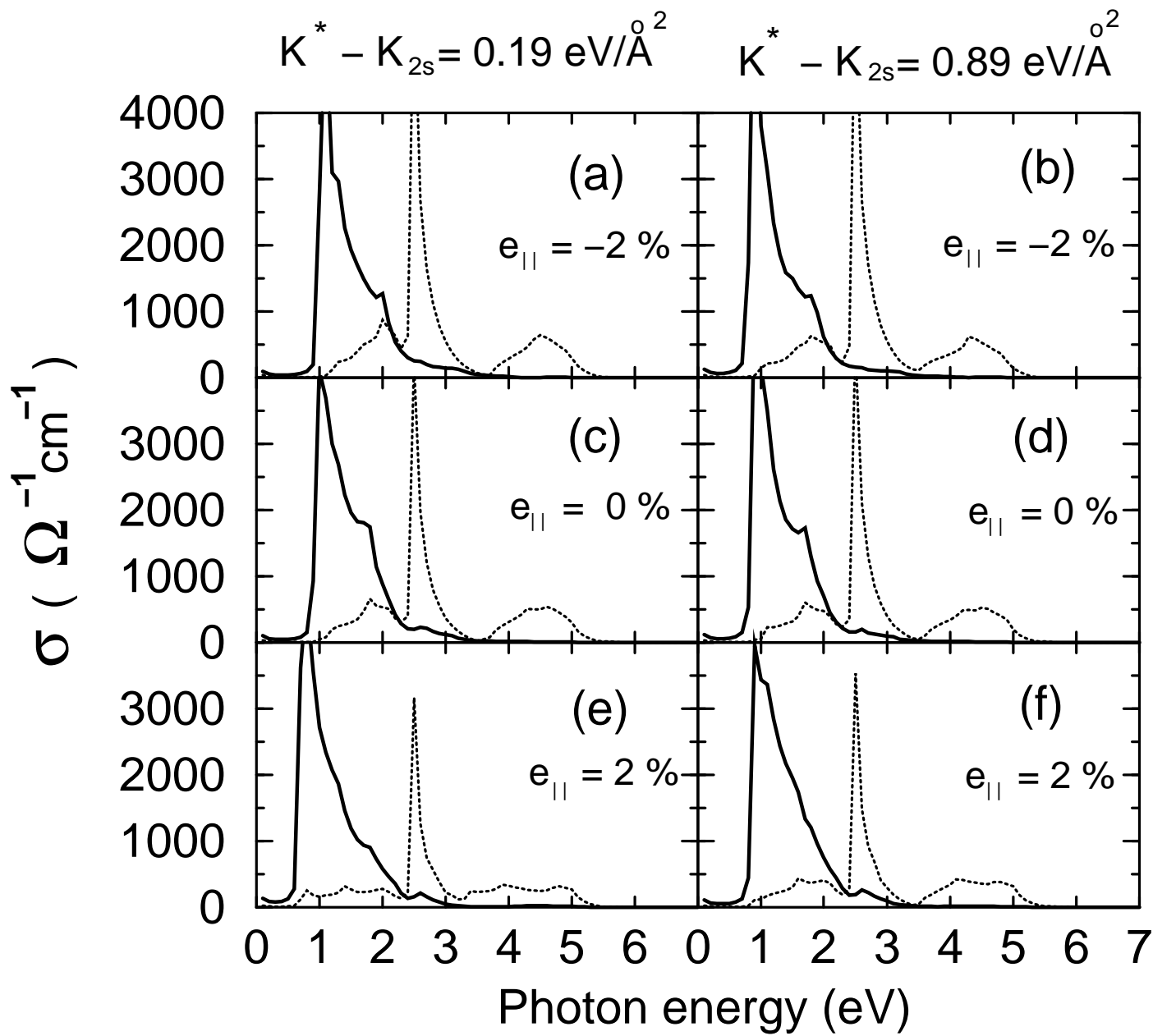


Fig. 8, Ahn and Millis

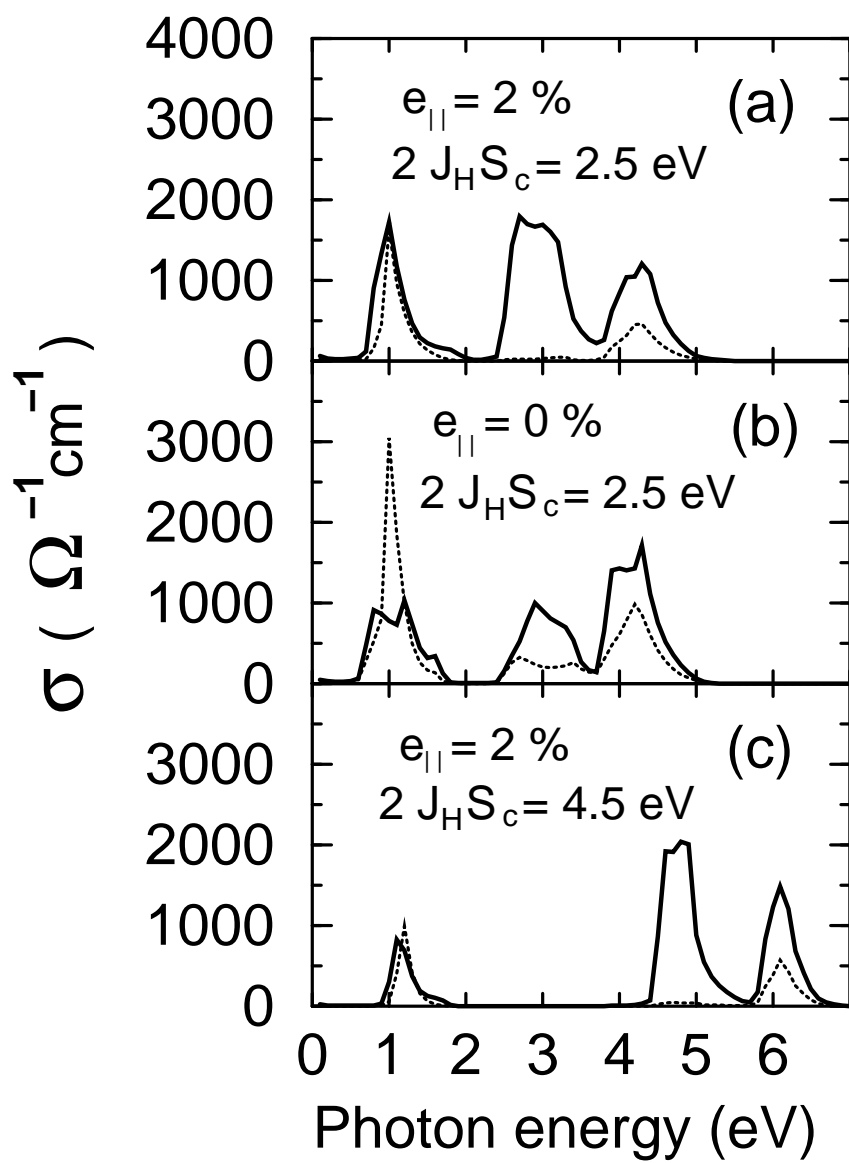


Fig. 9, Ahn and Millis